AEDC-TR-71-83

cy/

LOW-DENSITY SUPERSONIC SPHERE DRAG WITH VARIABLE WALL TEMPERATURE

D. L. Whitfield and H. K. Smithson
ARO, Inc.

July 1971

Approved for public release; distribution unlimited.

VON KÁRMÁN GAS DYNAMICS FACILITY
ARNOLD ENGINEERING DEVELOPMENT CENTER
AIR FORCE SYSTEMS COMMAND
ARNOLD AIR FORCE STATION, TENNESSEE

NOTICES

LOW-DENSITY SUPERSONIC SPHERE DRAG WITH VARIABLE WALL TEMPERATURE

D. L. Whitfield and H. K. Smithson
ARO, Inc.

FOREWORD

This work was sponsored by the Air Force Cambridge Research Laboratories (AFCRL) (CRMP), Bedford, Massachusetts, under Program Element 65701F, Project 6682.

The results presented were obtained by ARO, Inc. (a subsidiary of Sverdrup & Parcel and Associates, Inc.), contract operator of the Arnold Engineering Development Center (AEDC), Air Force Systems Command (AFSC), Arnold Air Force Station, Tennessee, under Contract F40600-71-C-0002. This work was conducted intermittently from December 1969 to September 9, 1970, under ARO Project No. VQ0938. The manuscript was submitted for publication on February 25, 1971.

The authors wish to acknowledge M. H. Jones (now at North Carolina State University) for writing the data reduction programs for both the drag data and tunnel calibration. Also, appreciation is due K. R. Kneile and H. N. Glassman, Central Computer Operations, ARO, Inc., for obtaining the numerical solutions to Eq. (8).

This technical report has been reviewed and is approved.

Emmett A. Niblack, Jr.	Joseph R. Henry
Lt Colonel, USAF	Colonel, USAF
AF Representative, VKF	Director of Test
Directorate of Test	

ABSTRACT

Force measurements were made to investigate the effect of wall temperature on sphere drag in low-density supersonic flow. Drag data were obtained by fixing flow conditions and changing only the sphere wall temperature. Conditions covered in the experiment include $3.3 < M_\infty < 3.7$, $4.0 < Re_\infty < 10.0$, $0.5 < Kn_\infty < 1.3$, and $1.2 < T_W/T_\infty < 3.0$. A means of correlating drag data in transition flow is suggested, and its validity assessed by applying the correlation parameter to this and several other sets of experimental data.

CONTENTS

APPENDIXES

I. ILLUSTRATIONS

NOMENCLATURE

A	Cross-sectional area of sphere, πr^2
C_D	Drag coefficient, $D/(1/2\ \rho_\infty U_\infty{}^2 A)$
C_p	Specific heat of gas at constant pressure
C_v	Specific heat of gas at constant volume
D	Drag
d	Sphere diameter
erf(x)	Error function, $(2/\sqrt{\pi}) \int_0^x e^{-t^2}\, dt$
f	Velocity distribution function
g	Relative speed of molecules
H	Local total enthalpy
h	Defined by Eq. (5e)
I	Defined by Eq. (8)
Kn	Knudsen number based on sphere diameter, λ/d
$\overline{K}_{w,d}$	$Kn_\infty/(\sqrt{\pi}\, S_w + 1)$

M	Mach number
m	Mass of a molecule
N	Collision frequency
n	Number density of molecules
p	Pressure
p_o'	Total pressure immediately downstream of a normal shock
p_p	Measured pitot pressure
q	Dynamic pressure, $\rho U^2/2$
R	Gas constant
Re	Reynolds number based on sphere diameter
$Re_{o,r*}$	Nozzle reservoir Reynolds number, $\rho_o \sqrt{2H_o}\, r^*/\mu_o$
Re_∞	$\rho_\infty U_\infty d/\mu_\infty$
r	Radius of sphere
r*	Nozzle throat radius
S	Speed ratio, $U/(2RT)^{1/2}$
S_r	$U_\infty/(2RT_r)^{1/2}$
S_w	$U_\infty/(2RT_w)^{1/2}$
S_∞	$U_\infty/(2RT_\infty)^{1/2}$
T	Temperature
T_r	Reference temperature, $(T_o^- + T^+)/2$
t	Time
U	Velocity
u	Molecular velocity component
v	Molecular velocity component
$\bar{v}$	Mean molecular velocity
w	Molecular velocity component
β	Angle defined in Fig. 5
γ	Ratio of specific heats, C_p/C_v

ζ	Defined by Eq. (5c)
η	Defined by Eq. (5b)
λ	Mean free path
μ	Viscosity
ξ	Defined by Eq. (5a)
ρ	Gas mass density
σ	Effective molecular diameter, $(T_2/T_1)^{1/2}$ or $(T_w/T_\infty)^{1/2}$

SUBSCRIPTS

1	Corresponding to class 1 molecules
2	Corresponding to class 2 molecules
d	Corresponding to sphere diameter
fm	Free-molecular value
o	Reservoir (total) condition
w	Sphere wall condition
∞	Free-stream condition

SUPERSCRIPTS

-	Denotes incoming molecules
+	Denotes outgoing molecules

SECTION I
INTRODUCTION

An extensive experimental sphere drag investigation has recently been completed by Bailey and Hiatt (Ref. 1) in an aeroballistic range of the von Kármán Gas Dynamic Facility (VKF) at AEDC. This test was conducted to obtain sphere drag coefficients for data reduction of the falling balloon experiments (Ref. 2). Their measurements covered a Mach number range of $0.12 < M_\infty < 6.39$ and Reynolds number range of $15 < Re_\infty < 50,300$ at a T_W/T_∞ ratio of about one. Sphere drag measurements were also made in the Aerospace Research Chamber (10V) of VKF as a part of this program. The 10V data are reported herein, and they cover the flow conditions $3.31 \leq M_\infty \leq 3.63$, $4.17 \leq Re_\infty \leq 9.27$, $0.55 \leq Kn_\infty \leq 1.29$, and $1.20 \leq T_W/T_\infty \leq 2.85$. In addition, the nominal Mach seven (M7) balance data reported in Ref. 3 were reduced using the present data reduction computer program. These data were previously reduced by hand calculations. The results are changed less than ±2 percent. The flow conditions of the M7 data are $7.21 \leq M_\infty \leq 7.77$, $2.85 \leq Re_\infty \leq 8.32$, $1.39 \leq Kn_\infty \leq 3.77$, and $3.90 \leq T_W/T_\infty \leq 5.44$.

The primary objective of the 10V investigation was to study the effect of wall temperature on sphere drag for Knudsen numbers of order one, O(1). A difficulty in investigating the effect of T_W is that the effect of other flow variables must be either known or eliminated. Unfortunately, the flow conditions required to produce $Kn_\infty \sim O(1)$ for practical model sizes (in this case d = 0.25 in.) are difficult to calibrate. This is due to the orifice effect, thermal transpiration effect, and viscous correction on pitot pressure measurements, as well as problems associated with calibrating a device to measure pressures near 10 μ Hg.

In addition to flow calibration a certain amount of difficulty is involved in measuring small drag forces (in this case the drag was on the order of 100 mg). The tare force on the balance sting must also be measured and subtracted from the total force measurement. The tare force was typically from 30 to 35 percent of the total drag force. Force measurements of this magnitude are sensitive to vibrations, balance alignment, and thermal environment, any one of which can cause meaningless drag measurements if not controlled. Obviously, interference and mechanical problems are removed when free-flight techniques are used; however, error is introduced in free-flight data by inaccuracies in the sphere position measurements. The probable magnitude of error and scatter increases as more rarefied drag measurements are made (e. g., see Refs. 1, 4, and 5). If the experimental scatter is greater than the effect of T_w, or if sufficient data points are not obtained in order to apply a statistical analysis, free-flight data are difficult to interpret as to the effect of T_w only. Furthermore, the models are usually small and made of lightweight materials having low thermal conductivity. Thus, the accuracy of determining their mass and the effective wall temperature experienced by the molecules decreases. In view of the advantages and disadvantages of the balance and free-flight techniques, and because a suitable drag balance was available (Ref. 5), the balance technique was chosen for this investigation.

A discussion of the appropriate dynamic simulation parameters for hypervelocity bluff body drag coefficients has been given by Potter and Miller (Ref. 6). Because some of the data to be considered here correspond to low supersonic Mach numbers, another expression for correlating sphere drag data will be derived and its validity assessed in conjunction with an approximate analysis presented in Refs. 3 and 7. Comparisons of several sets of experimental data with the approximate theory will be made.

SECTION II
EXPERIMENTAL FACILITY AND NOZZLE CALIBRATION

The 10V chamber of the Aerospace Division of VKF is a cryogenically pumped chamber 10 ft in diameter and 20 ft in length. It has about an 8-ft-diam and 10-ft-long internal working volume when the nominal Mach three (M3) or Mach six (M6) nozzle is installed for operation as a wind tunnel. The principal pumping capacity of the 10V for this test was provided by 620 ft^2 of 77°K liquid-nitrogen (LN_2) cryosurfaces and 240 ft^2 of 15 to 20°K gaseous-helium (GHe) cryosurfaces. Although 8 kw is available, only a 4-kw GHe refrigeration capacity was used. This arrangement permitted the continuous pumping of 8 to 10 gm/sec of nitrogen (or argon) at a chamber pressure of about 10^{-4} mm Hg.

The 10V instrumentation and hardware arrangement was the same for this test as described in Ref. 3. A schematic of the chamber is given in Fig. 1 (Appendix I). The balance used to measure the drag force is described in detail in Ref. 5. Problems associated with balance alignment, vibration damping, thermal control, and calibration (all of which were accomplished remotely in the 10V environment) are also discussed in Ref. 5.

Drag measurements were made on the centerline, 10 in. downstream of the exit plane of the M3 nozzle. The flow was calibrated at this point using a 1-in.-diam, 10-deg internally chamfered pitot probe. An MKS Baratron® (variable capacitance transducer) was used to measure both the total pressure, p_o, and the pitot pressure, p_p. Three corrections to pitot pressure measurements in this flow regime were considered: (1) thermal transpiration effect, (2) orifice effect, and (3) viscous correction. The thermal transpiration correction was found to be negligible. Following the method of Kinslow and Potter (Ref. 8) the orifice effect was found to contribute less than one percent change in measured pressure and therefore was neglected. The external-flow viscous correction to the impact pressure, however, was a large as 10 percent and therefore not negligible. The viscous correction data presented in Ref. 3 were used to correct the pitot measurements. These data were curve fitted and a computer program written to carry out the necessary iterations for data reduction.

The criterion described in Ref. 3 for merged flow, i. e., the boundary layer completely filling the nozzle, was used here. The reservoir Reynolds number based on throat radius ($Re_{o,r*}$, see Ref. 9) for merged flow in the M3 nozzle is $Re_{o,r*} < 1000$. No data are presented for $Re_{o,r*} < 1000$.

The axial M_∞ gradient 10 in. downstream of the conical M3 nozzle is about 0.015 per inch. For the flow conditions of these measurements, this corresponds to a free-stream dynamic pressure gradient from 1.2 to 1.3 percent per inch. The effect of this gradient on C_D for a 0.25-in.-diam sphere was therefore negligible.

SECTION III
DATA ACQUISITION

The data acquisition procedure was somewhat different than commonly used to make drag measurements in the transition regime. Usually flow conditions are established and force measurements are made using different model sizes, thereby obtaining C_D for various Kn_∞ or Re_∞ at about constant T_w/T_∞. Or, a given model is used and p_o varied to obtain C_D versus Kn_∞. Then, other flow variables, such as T_o, are changed, and similar data are acquired. The requirement of large Kn_∞, or small Re_∞, restricts the model in most facilities to a size such that T_w cannot be varied conveniently, and frequently it is difficult to measure at all. Since free-stream mean free paths, λ_∞, on the order of an inch can be produced in the 10V, sufficiently large models can be used such that T_W can be varied and continuously monitored. Therefore, by fixing flow conditions and model size, drag data can be obtained which produce vertical lines on a plot of C_D versus Kn_∞, or Re_∞, since each data point is associated with a different T_W/T_∞.

The standard procedure for making these drag measurements was to cool the sphere to some temperature, establish flow conditions, and then periodically make force measurements as the sphere temperature increased due to convective heating of the sphere by the flowing gas. Since the chamber pressure was typically about 10^{-7} mm Hg when there was no flow into the chamber, there was insufficient gas density to decrease the sphere temperature below about 270°K even though there are 77°K and 15-20°K cryopanels in the chamber. Also radiation heat transfer would not decrease the sphere temperature below 270°K when the sphere was located in the center of the chamber. Therefore, a means of convective heat transfer was supplied to the chamber by a 1.3×10^{-3} cc/sec (standard) calibrated helium leak to raise the chamber pressure to about 10^{-3} mm Hg. Since 15°K surfaces will not effectively pump helium, the helium will stay in the chamber until removed by diffusion pumps, and thereby the medium necessary for convective cooling of the sphere could be maintained as long as required. Unfortunately, because of the time required to establish flow conditions and make a force measurement, the lowest T_W at which data were taken was about 210°K. The largest value of T_W attainable was limited by radiation to the cryopanels. For the higher T_O data the largest T_W attained was about 390°K. Typical rates of increase of T_W are shown in Fig. 2.

A second 0.25(±0.0002)-in.-diam aluminum sphere, identical to the one used on the balance sting to measure the drag, was used to determine the sphere wall temperature. This second sphere was supported by the leads to a thermocouple which was used to measure the sphere temperature. It was attached to the same support as the balance and was simultaneously subjected to the same flow conditions as the sphere mounted on the balance sting. From the time-dependent solution for heat transfer in a sphere (Ref. 10), the temperature at the thermocouple was calculated to be within one percent of the surface temperature in less than two seconds. This lag was therefore negligible, and the thermocouple reading was taken as T_W.

The method used to reduce and determine tare forces was the same as that described and illustrated in Ref. 3. Tare forces for these measurements varied from a minimum of 27 percent for the T_O = 300°K data to a maximum of 38 percent for the T_O = 755°K data. An example of the force and pitot pressure measurements is given in Fig. 3.

SECTION IV
EXPERIMENTAL RESULTS

Drag measurements were made at three different reservoir temperatures of nominally 300, 640, and 750°K. These data are tabulated in Table I (Appendix II) and presented in the form of C_D versus Re_∞ in Fig. 4. The drag data definitely illustrate a "grouping" with T_o when presented in this form. However, it should be noted that each group of T_o data has associated with it a different range of flow conditions, and hence each T_o group has a different $C_{D_{fm}}$ limit which it is assumed to approach asymptotically. ($C_{D_{fm}}$ is herein based on complete accommodation and diffuse reflection.) For these data the M_∞ and T_w/T_∞ ranges associated with each T_o group maximize the difference in the $C_{D_{fm}}$ limit. For example, the T_o = 300°K data have the lowest values of M_∞ and the largest values of T_w/T_∞, each contributing to increasing $C_{D_{fm}}$, whereas the $T_o \approx$ 750°K data have the largest values of M_∞ and lowest values of T_w/T_∞, each contributing to decreasing $C_{D_{fm}}$. Therefore, it is appropriate to consider the normalization of the drag data by the $C_{D_{fm}}$ value associated with each data point. The results of such a normalization will be presented subsequently.

Obviously, the normalization of C_D by $C_{D_{fm}}$ is sufficient for correlating free-molecular drag data if the theory used to calculate $C_{D_{fm}}$ is valid. However, these drag data correspond to Kn_∞ of order one and therefore are subject to the physics of the more complicated transition regime. Since no general solution has been found for the Boltzmann equation which describes the flow about a body in this regime, the appropriate parameters for correlating these drag data are not available. Fortunately, approximate solutions of the Boltzmann equation and solutions to approximate models of transition flow have exposed useful parameters. A summary of most of the parameters applicable to hypersonic flows is given by Potter and Miller (Ref. 6). Attention will be given here to correlating supersonic drag data. A new correlation parameter will be derived and its validity investigated by using it to correlate these as well as other drag data. Although the purpose of this report is not to derive and assess various correlation parameters, the use of a parameter to correlate these data is important since variables which can affect sphere drag in this regime change for each data point in the present experiment.

SECTION V
CORRELATION PARAMETER

The Knudsen number, $Kn_w = \lambda_w/d$, based on the mean distance traveled by molecules emitted from the surface of a body before experiencing a collision with free-stream molecules, has been shown in various theoretical sphere drag investigations (Refs. 7 and 11 through 16) to be of importance. The derivations of λ_w have assumed that the emitted molecules travel at some average velocity, and in some instances λ_w is restricted to cold-wall, high-Mach-number conditions. It is of interest, therefore, to consider fundamentally the derivation of λ_w and to determine whether or not a more accurate expression for λ_w can be obtained without formidable mathematical difficulties.

Consider two classes of smooth, rigid, elastic, spherical molecules denoted as 1 and 2. For such molecules no problem exists concerning the concept of a free path since the molecules affect each other's motion only at collisions. Following the development of Chapman and Cowling (Ref. 17), the total number of collisions occurring per unit volume and unit time between pairs of molecules of class 1 with class 2 is given by

$$N_{12} = \iiiint\!\!\iint \pi g \sigma_{12}^2 \; f_1 f_2 \, du_1 \, dv_1 \, dw_1 \, du_2 \, dv_2 \, dw_2 \tag{1}$$

where

$$g = [(u_1 - u_2)^2 + (v_1 - v_2)^2 + (w_1 - w_2)^2]^{1/2} \tag{2}$$

and

$$\sigma_{12} = \frac{1}{2}(\sigma_1 + \sigma_2) \tag{3}$$

In Eq. (3), σ_1 and σ_2 are the diameters of the molecules of class 1 and class 2, and f_1 and f_2 are the distribution functions of class 1 and class 2. For the coordinate system shown in Fig. 5, N_{12} becomes, after nondimensionalizing,

$$N_{12} = \int_{-\infty}^{\infty}\int_{-\infty}^{\infty}\int_{-\infty}^{0}\int_{-\infty}^{\infty}\int_{-\infty}^{\infty}\int_{0}^{\infty} \frac{2\pi \sigma_{12}^2 \, n_1 n_2 \sqrt{2RT_1}}{\pi^3} h \times$$

$$e^{-[(\xi_1 - S_1 \sin\beta)^2 + (\eta_1 + S_1 \cos\beta)^2 + \zeta_1^2] - (\xi_2^2 + \eta_2^2 + \zeta_2^2)} \, d\xi_1 d\eta_1 d\zeta_1 d\xi_2 d\eta_2 d\zeta_2 \tag{4}$$

where

$$\xi_i = \frac{u_i}{\sqrt{2RT_i}} \tag{5a}$$

$$\eta = \frac{v_i}{\sqrt{2RT_i}} \tag{5b}$$

$$\zeta_i = \frac{w_i}{\sqrt{2RT_i}} \tag{5c}$$

$$S_1 = \frac{U_1}{\sqrt{2RT_1}} \tag{5d}$$

$$h = [(\xi_1 - \tau\xi_2)^2 + (\eta_1 - \tau\eta_2)^2 + (\zeta_1 - \tau\zeta_2)^2]^{1/2} \tag{5e}$$

$$\tau = (T_2/T_1)^{1/2} \tag{5f}$$

and i may take on the values 1 or 2. Note the additional 2 as a coefficient in the integrand of Eq. (4). This 2 is required in order to satisfy continuity since the limits of ξ_2 are $-\infty$ to 0, and hence only one half of the molecules emitted from the surface element in Fig. 5 would otherwise be accounted for. The mean distance traveled by molecules of class 2 between successive collisions with those of class 1 is given by (cf. Ref. 17)

$$\lambda_{21} = \frac{n_2 \bar{v}_2}{N_{12}} \tag{6}$$

where $\bar{v}_2$ is the mean speed of class 2 molecules. Taking $\bar{v}_2 = (9\pi RT_2/8)^{1/2}$ (Ref. 13), $\lambda_{11} = (\sqrt{2}\,\pi n_1 \sigma_{11}{}^2)^{-1}$ (Ref. 17), and $\sigma_1 = \sigma_2$ (since the same size molecules are being considered and no dependence of σ on temperature is assumed at this point), one obtains

$$\frac{\lambda_{21}}{\lambda_{11}} = \frac{3\sqrt{2\pi}\;\pi^3}{8}\,\frac{\tau}{I} \tag{7}$$

where

$$I = \int_{-\infty}^{\infty}\int_{-\infty}^{\infty}\int_{-\infty}^{0}\int_{-\infty}^{\infty}\int_{-\infty}^{\infty}\int_{0}^{\infty} h\, e^{-[(\xi_1 - S_1\sin\beta)^2 + (\eta_1 + S_1\cos\beta)^2 + \zeta_1{}^2 + \xi_2{}^2 + \eta_2{}^2 + \zeta_2{}^2]}\, d\xi_1 d\eta_1 d\zeta_1 d\xi_2 d\eta_2 d\zeta_2 \tag{8}$$

and h is given by Eq. (5e).

The integral I given by Eq. (8) has not been integrated in closed form. Approximate results have been obtained for Eq. (7) by replacing g in Eq. (1) by the relative mean speeds of the class 1 and 2 molecules, see, e. g., Ref. 18. The resulting expression has been used for the mean free path of emitted molecules from a surface in several theoretical investigations, e. g., Refs. 7, 11, 13, and 15. Of course the accuracy of this approximation can only be determined by comparison with exact solutions of Eq. (8). Even numerical solutions to Eq. (8) are rather difficult and would require a good deal of computer time for accurate results for the several values of τ, S_1 and β which should be investigated. In view of this, it is of interest to present another approximate solution to Eq. (8) which will be shown to be in reasonable agreement with the numerical solutions of Eq. (8) which have been obtained. Also, this approximate solution will provide an upper bound for $\lambda_{21}/\lambda_{11}$ (Eq. (7)), whereas the approximate result given by using mean speeds for g in Eq. (1) provides a lower bound for $\lambda_{21}/\lambda_{11}$ when compared to the numerical solutions.

Consider the integrand of Eq. (8). Notice that it is non-negative and attains its larger values at relatively small values of independent variables ζ_1, ξ_2, η_2, and ζ_2 because of the exponential term. Because of the terms $(\xi_1 - S_1 \sin\beta)$ and $(\eta_1 + S_1 \cos\beta)$ in the exponential, the integrand will attain its larger values for ξ_1 near $(S_1 \sin\beta)$ and η_1 near $(-S_1 \cos\beta)$. It appears that in rarefied flow, molecules emitted near β of $\pi/2$ have more effect on sphere drag than those emitted at locations remote from the stagnation point. Therefore, Eq. (8) will be considered for the case $|S_1 \sin\beta| >> |-S_1 \cos\beta|$. With $|S_1 \sin\beta| >> |-S_1 \cos\beta|$ the integrand of Eq. (8) is larger when ξ_1 is on the order of $S_1 \sin\beta$, because ξ_1 contributes more to increasing h before the exponential term dominates than do the other independent variables. The first term in h (Eq. (5e)) is therefore retained, and h is approximated by $h = \xi_1 - \xi_2\tau$. Of course ξ_2 will be small compared to ξ_1, when the integrand of Eq. (8) is very large (because the exponential term dominates when ξ_2 is large) and hence will contribute about the same as the terms dropped. However, notice that the integral of $(-\xi_2\tau)$ times the exponential is greater than zero because only negative values of ξ_2 are considered. Therefore, since the contribution of the integral of the terms which were dropped is greater than zero, then the approximation is slightly more accurate if $(-\xi_2\tau)$ is retained. The resulting integral is

$$I = \int_{-\infty}^{\infty}\int_{-\infty}^{\infty}\int_{-\infty}^{0}\int_{-\infty}^{\infty}\int_{-\infty}^{\infty}\int_{0}^{\infty}(\xi_1-\xi_2\tau)\times$$

$$e^{-[(\xi_1-S_1\sin\beta)^2+(\eta_1+S_1\cos\beta)^2+\zeta_1^2+\xi_2^2+\eta_2^2+\zeta_2^2]}d\xi_1 d\eta_1 d\zeta_1 d\xi_2 d\eta_2 d\zeta_2 \quad (9)$$

There is no problem in integrating Eq. (9), see, e. g., the Appendix of Ref. 19. The result is

$$I = \frac{\pi^2\sqrt{\pi}}{4}\left\{[1+\mathrm{erf}(S_1\sin\beta)]\,[\sqrt{\pi}S_1\sin\beta+\tau]+e^{-S_1^2\sin^2\beta}\right\} \quad (10)$$

Substituting Eq. (10) into Eq. (7) for I gives

$$\frac{\lambda_{21}}{\lambda_{11}} = \frac{3\pi\sqrt{2}\,\tau}{2\left\{[1+\mathrm{erf}(S_1\sin\beta)]\,[\sqrt{\pi}\,S_1\sin\beta+\tau]+e^{-S_1^2\sin^2\beta}\right\}} \quad (11)$$

Therefore, for $S_1 \sin\beta$ of order one and larger, Eq. (11) can be rather accurately approximated by

$$\frac{\lambda_{21}}{\lambda_{11}} = \frac{3\pi\sqrt{2}\,\tau}{4(\sqrt{\pi}\,S_1 \sin\beta + \tau)} \tag{12}$$

This result is applied to the problem at hand by considering the class 1 molecules to be free-stream molecules, $\lambda_{11} = \lambda_\infty$, and the class 2 molecules to be molecules emitted from the surface of the sphere, $\lambda_{21} = \lambda_w$. Then τ becomes $\sqrt{T_w/T_\infty}$. Using $S_1 = S_\infty$, $S_w = S_\infty / \sqrt{T_w/T_\infty}$, and the approximation $\sin\beta = 1$, one obtains

$$\frac{\lambda_w}{\lambda_\infty} = \frac{3\pi\sqrt{2}}{4(\sqrt{\pi}\,S_w + 1)} \tag{13}$$

The adequacy of Eq. (13) is now assessed by comparisons with results using numerical solutions for I in Eq. (7). In view of Eq. (13), it appears more convenient to consider the reciprocal of λ_w/λ_∞ since at least the approximate solution is linear in S_w. Results obtained numerically, by the present approximation, and by using mean speeds for g in Eq. (1) are all presented in Fig. 6. The numerical solutions in Fig. 6 were obtained for $1/2 \leq \tau \leq 5$ which corresponds to $1/4 \leq T_w/T_\infty \leq 25$ for each S_∞.

As mentioned previously, the approximate solutions provide upper and lower bounds to the numerical solutions for these values of the parameters τ and S_∞. It is of interest to note that the slopes of the approximate results are identical and correspond to about the mean slope of the numerical solutions for $S_\infty > 2$. Equation (13) is in better agreement with the numerical results as S_∞ becomes large, and since this regime is of more interest here (and in the approximate theoretical analysis where the other result has been used), it seems more appropriate to use Eq. (13), i. e., take

$$\frac{\lambda_w}{r} = \frac{3\pi\sqrt{2}\,Kn_\infty}{2(\sqrt{\pi}\,S_w + 1)} \sim \frac{Kn_\infty}{\sqrt{\pi}\,S_w + 1} \tag{14}$$

It should be noted that the result given in Eq. (13) is related to that of Ref. 13, i. e.,

$$\frac{(\lambda_w/\lambda_\infty)_{\text{Ref. 13}}}{(\lambda_w/\lambda_\infty)_{\text{Eq. (13)}}} = \frac{S_w\sqrt{\pi} + 1}{S_w\sqrt{\pi} + 2.35} \approx 1 \text{ when } S_w\sqrt{\pi} >> 1$$

Therefore, even though either approximation may be used, it has been found that use of Eq. (13) results in slightly better correlation of experimental data.

SECTION VI
THEORETICAL AND EXPERIMENTAL COMPARISONS

The more appropriate available sphere drag data with which to compare the present results are those of Potter and Miller (Ref. 6), Davis and Sims (Ref. 20), Smolderen, et al. (Ref. 21), and Whitfield and Stephenson (Ref. 3). Also, the lower density data of Bailey and Hiatt (Ref. 1) are considered. The data from these sources are compared with the present results in Figs. 7 through 10 in terms of several parameters. Figures 7 and 8 present the data in terms of the free-stream Reynolds and Knudsen numbers. Owing to the variations in M_∞ and T_w/T_∞, correlation of the results would not be expected. In Fig. 9 these data are presented with C_D normalized by $C_{D_{fm}}$, where $C_{D_{fm}}$ is calculated by using the particular S_∞ and T_w/T_∞ values associated with each data point. A further improvement is illustrated in Fig. 10 by using $Kn_\infty/(\sqrt{\pi}\, S_w + 1)$, from Eq. (14), in place of Kn_∞. The approximate theory in Fig. 10 was obtained by using λ_w/r given by Eq. (14) in the expression derived for the sphere drag coefficient in Ref. 7. The resulting equation is

$$\frac{C_D}{C_{D_{fm}}} = \frac{1}{1 + \dfrac{1}{\left(1 + \dfrac{3\pi\sqrt{2}}{2}\,\overline{K}_{w,d}\right)^2}} \tag{15}$$

where

$$\overline{K}_{w,d} = \frac{Kn_\infty}{\sqrt{\pi}\, S_w + 1} \tag{16}$$

The comparison between experiment and theory and experiment in Fig. 10 is reasonable for $\overline{K}_{w,d} > 10^{-1}$ considering that the experimental results consist of data over an M_∞ range from 2.5 to 8.3 and a T_w/T_∞ range from 0.8 to 15. Also, the measurements made by Davis and Sims (Ref. 20) were taken in a carbon dioxide (CO_2) gas, whereas the other measurements were made in nitrogen and air. Although the range data of Bailey and Hiatt (Ref. 1) do not overlap the conditions of the present measurements, the comparison in Fig. 10 illustrates that their data are in agreement with the data of Potter and Miller (Ref. 6), Davis and Sims (Ref. 20), and the theory; all three of which are in good agreement and represent about the mean drag value of the present data.

Since slightly more accurate numerical solutions were obtained for λ_w/λ_∞ (Fig. 6), it is of interest to determine the changes attributable to using numerical values of λ_w/λ_∞ in place of Eq. (13). In order to do this, a mean linear curve was placed through the appropriate range of conditions in Fig. 6 corresponding to the data in Fig. 10, and the equation of the linear curve was determined. As a result, λ_∞/λ_w was proportional to $(S_w + 1)$ and therefore $\lambda_w/r \sim Kn_\infty/(S_w + 1)$. Figure 11 represents the correlation provided by the numerical solutions for the same data considered in Figs. 7 through 10. The approximate theory was obtained by substituting the linear equation for λ_w/r obtained from the numerical solutions into the sphere drag expression of Ref. 7. Close examination of Fig. 11 indicates that little change in the correlation was obtained.

A more critical comparison between theory and the variation of the present drag data with T_w is provided by Fig. 12. Data used for this comparison are those taken at essentially constant M_∞ and Kn_∞, and therefore any change in drag should be due only to a change in T_w. For constant M_∞ and Kn_∞ the theoretical C_D of Ref. 7 depends only on T_w/T_∞, and hence curves of constant M_∞ and Kn_∞ can be constructed for comparison in Fig. 12. The experimental data and theory have almost identical slopes in Fig. 12, and the comparison is considered good. Also, the variation of the present data and theory with T_w/T_∞ in Fig. 12 is further substantiated by the data of Potter and Miller (Ref. 6), Davis and Sims (Ref. 20), and Bailey and Hiatt (Ref. 1). The variation of the present drag data with S_w is compared with theory in Fig. 13.

Calculated values of C_D from Eq. (15) (at constant M_∞ with $\gamma = 1.4$ and $T_w/T_\infty = 1$) are presented as a function of Re_∞ in Fig. 14. With $\gamma = 1.4$ and $T_w/T_\infty = 1$, Eq. (15) can be written in terms of M_∞ and Re_∞ for $M_\infty \geq 2.5$ and $\lambda_\infty = (\pi/2RT_\infty)^{1/2}\,\mu_\infty/\rho_\infty$, viz.,

$$C_D = \frac{2.000 + \dfrac{1.412}{M_\infty} + \dfrac{2.857}{M_\infty{}^2}}{1 + \dfrac{1}{\left(1 + \dfrac{9.935\,\dfrac{M_\infty}{Re_\infty}}{1.483\,M_\infty + 1}\right)^2}} \tag{17}$$

This C_D is not valid for continuum flow since the drag becomes insensitive to T_w at high densities, and $C_D/C_{D_{fm}}$ limits are usually something other than one-half as $Kn_\infty \rightarrow 0$. However, it has been shown to be valid through the transition regime to the slip flow regime

(Ref. 22). In terms of limits, Eq. (15), and hence Eq. (17), can be used for $\bar{K}_{w,d} = Kn_\infty/(\sqrt{\pi}\, S_w + 1) > 0.1$ or $\bar{K}_{r,d} = Kn_\infty/(\sqrt{\pi}\, S_r + 1) > 0.1$. For the conditions of the present experiment at $M_\infty \approx 3$, this implies $Re_\infty < 0(10)$.

Although hypersonic cold-wall data are not of prime importance here, they become of interest when considered for correlation of data such as used in Figs. 7 through 10. A plot of several sets of high enthalpy (H_o) hypersonic data (Refs. 6, 13, 21, and 23 through 25) in terms of $\bar{K}_{w,d}$ (Fig. 15, open symbols) reveals that the cold-wall data have larger values of $C_D/C_{D_{fm}}$ at the same values of $\bar{K}_{w,d}$ than the lower M_∞ and/or lower H_o data considered in Figs. 7 through 10. Although it is only speculation at this point, an explanation might be that the energy of the gas molecules on the outermost surface of the sphere is rapidly increased above that corresponding to T_w by collisions with the high energy free-stream molecules. If this is the case, an increase in drag occurs because of the higher momentum (pressure) exerted on the body by the molecules which leave the surface. The work of Kinslow and Potter (Ref. 8) does not address this problem specifically; however, it is considered in search of an estimate of this effect.

Kinslow and Potter (Ref. 8) used a two-sided Maxwellian distribution function to describe the gas in the vicinity of a surface. For a bluff body stagnation region their expression for the surface pressure p_w is approximated by

$$\frac{p_w}{p_{i_{fm}}} \approx \left(\frac{T_r}{T_w}\right)^{1/2} \tag{18}$$

where $p_{i_{fm}} = mn^- RT^- (T_w/T^-)^{1/2}$ is the pressure in a cavity in the surface where the cavity orifice is much smaller than the mean free path in the cavity, and the reference temperature T_r is defined as

$$T_r = \frac{T_o^- + T^+}{2} \tag{19}$$

The minus superscript denotes incoming molecules and the plus superscript denotes outgoing molecules. The present approximation made in Eq. (18) is the use of the exponent 1/2 instead of the more accurate value which may vary between approximately 1/2 and 1/(2.3). Since $p_{i_{fm}}$ is proportional to $(T_w)^{1/2}$, the actual surface pressure p_w is given approximately by replacing T_w with T_r in $p_{i_{fm}}$.

It seems appropriate to investigate the change in the normalized drag data caused by using T_r in place of T_w in determining the pressure attributable to emitted molecules in calculating $C_{D_{fm}}$. The reference temperature, T_r, was used to calculate both $C_{D_{fm}}$ and $\overline{K}_{r,d}$ (i. e., $\overline{K}_{r,d} = Kn_\infty/(\sqrt{\pi}\, S_r + 1)$) in Fig. 15 (closed symbols). The solid curve in Fig. 15 is given by Eq. (15). As a result, for the data considered in Figs. 7 through 10, $T_r \approx T_w$, and quite good correlation of all the data is obtained by using T_r. Moreover, the scatter in the data of a given set is decreased somewhat; note particularly the $17.43 \leq M_\infty \leq 21.00$ data of Ref. 6.

Obviously, the argument presented for the use of T_r for correlating drag data is not rigorous. At this point the only justification for its use is that apparently it works. It should be pointed out that Kinslow and Potter (Ref. 8) showed that the existing data associated with the so-called orifice effect can be correlated using T_r to calculate a Knudsen number based on the orifice diameter. The physics behind the usefulness of T_r for correlating drag data should be investigated further.

SECTION VII
CONCLUSIONS

The present drag data for constant T_o are correlated quite well by the parameter used in Fig. 10 (the symbol and T_o correspondence is identified in Fig. 4); however, there is a two- to four-percent difference in the drag coefficients of the three groups of constant T_o data. Probably the most plausible explanation for this discrepancy is the presence of small errors. Possible errors which are considered to contribute less than one-percent change in the results are (1) thermal transpiration correction to measured p_o, (2) error involved in measuring T_o, (3) zero shift of drag balance caused by thermal environment, and (4) inaccuracy in positioning the balance and pitot probes. A more likely source of error is introduced by the actual flow calibration. The necessary corrections to the pitot pressure measurements increase with T_o to a maximum of about 10-percent correction at T_o = 755°K. It is entirely possible that a combination of the smaller errors mentioned above, errors in actually measuring pitot pressures, and errors introduced by the corrections applied to the pitot pressures could account for the two- to four-percent variation in $C_D/C_{D_{fm}}$ among the three T_o groups.

It should be kept in mind, however, that the total deviation of the present data is on the order of the scatter in existing free-flight data in this regime acquired supposedly at constant flow conditions. Moreover, the mean of all the present data is shown in Fig. 10 to be in good agreement with available experimental data. The scatter among the presented data at constant T_o is less than ±1 percent (Ref. 3), and the variation or slope of C_D with T_w (Fig. 12) is considered accurate within one percent.

The parameter provided by Eq. (14) is useful in correlating a class of sphere drag data for $\bar{K}_{w,d} > 0.01$ and low total enthalpy. Equation (15) is shown in Fig. 10 to be in rather good agreement with the data of prime interest.

REFERENCES

1. Bailey, A. B. and Hiatt, J. "Free-Flight Measurements of Sphere Drag at Subsonic, Transonic, Supersonic, and Hypersonic Speeds for Continuum, Transition, and Near Free-Molecular Flow Conditions." AEDC-TR-70-291, March 1971.

2. Engler, N. A. "Development of Methods to Determine Winds, Density, Pressure, and Temperature from the Robin Falling Balloon." University of Dayton Research Institute Report No. AF19(604)-7450, AFCRL-65-448, May 1965.

3. Whitfield, D. L. and Stephenson, W. B. "Sphere Drag in the Free-Molecular and Transitional Flow Regimes." AEDC-TR-70-32 (AD704122), April 1970.

4. Bailey, A. B. "High-Speed Sphere Drag in the Transition-Flow Regime in an Aeroballistic Range." Rarefied Gas Dynamics, Vol. II, Academic Press, New York, 1967, pp. 1127-1143.

5. Stephenson, W. B. and Whitfield, D. L. "Drag Measurement in a Low Density Gas Stream." AEDC-TR-70-25 (AD705576), May 1970.

6. Potter, J. L. and Miller, J. T. "Consideration of Simulation Parameters for Blunt Thick Bodies in Rarefied High-Speed Flows." AEDC-TR-68-242 (AD678159), November 1968.

7. Whitfield, D. L. "Analysis of Sphere and Cylinder Drag in Rarefied Flow." Presented at 7th International Symposium on Rarefied Gas Dynamics, June 29 – July 3, 1970, Pisa, Italy.

8. Kinslow, M. and Potter, J. L. "Reevaluation of Parameters Relative to the Orifice Effect." Presented at 7th International Symposium on Rarefied Gas Dynamics, June 29 – July 3, 1970, Pisa, Italy.

9. Rae, W. J. "Some Numerical Results on Viscous Low-Density Nozzle Flows in the Slender-Channel Approximation." AIAA Paper 69-654, June 1969.

10. Carslaw, H. S. and Jaeger, J. C. Conduction of Heat in Solids. Oxford: Clarendon Press, Second Edition, 1959.

11. Perepukhov, V. A. "Aerodynamic Characteristics of a Sphere and Blunt-Nosed Cone in a Highly Rarefied Gas Flow." (Translated from Russian) FTD-MT-24-135-68 (AD681686), 1967.

12. Willis, D. R. "On the Flow of Gases under Nearly Free Molecular Conditions." Princeton University Aero. Eng. Report No. 442, December 1958.

13. Kinslow, M. and Potter, J. L. "The Drag of Spheres in Rarefied Hypervelocity Flow." AEDC-TR-62-205 (AD290519), December 1962.

14. Probstein, R. F. "Shock Wave and Flow Field Development in Hypersonic Re-Entry." American Rocket Society. Paper presented at the ARS Semi-Annual Meeting, Los Angeles, California, May 9-12, 1960.

15. Baker, R. M. L. and Charwat, A. F. "Transitional Correction to the Drag of a Sphere in Free Molecule Flow." The Physics of Fluids, Vol. 1, No. 2, March-April, 1958, pp. 73-81.

16. Rose, M. H. "Drag on an Object in Nearly-Free Molecular Flow." The Physics of Fluids, Vol. 7, No. 8, August 1964, pp. 1262-1269.

17. Chapman, S. and Cowling, T. G. The Mathematical Theory of Non-Uniform Gases. Cambridge University Press, Third Edition, 1970.

18. Jeans, J. H. Dynamical Theory of Gases. Cambridge, Fourth Edition, 1925. (Also Dover Publication 1954.).

19. Patterson, G. N. "Molecular Flow of Gases." John Wiley & Sons, Inc., New York, Chapman & Hall, Limited, London, 1956.

20. Davis, T. C. and Sims, W. H. "An Experimental Study of the Drag of Simple Bodies in Rarefied Flow." Lockheed Missiles and Space Company Report, TM 54/20-166, LMSC/HREC A784888, November 1967.

21. Smolderen, J. J., Wendt, J. F., Naveau, J., and Bramlette, T. T. "Sphere and Cone Drag Coefficients in Hypersonic Transitional Flow." Rarefied Gas Dynamics, Vol. 1, Academic Press, New York, 1969, pp. 903-907.

22. Shidlovskiy, V. P. Introduction to Dynamics of Rarefied Gases. American Elsevier Publishing Company, Inc., New York, 1967.

23. Kussoy, M. I., Stewart, D. A., and Horstman, C. C. "Sphere Drag in Near-Free-Molecule Hypersonic Flow." AIAA Journal, Vol. 8, No. 11, November 1970, pp. 2104-2105.

24. Kussoy, M. I. and Horstman, C. C. "Cone Drag in Rarefied Hypersonic Flow." AIAA Journal, Vol. 8, No. 2, February 1970, pp. 315-320.

25. Phillips, W. M., Keel, A. G., Jr., and Kuhlthau, A. R. "The Measurement of Sphere Drag in a Rarefied Gas Using a Magnetic Wind Tunnel Balance." University of Virginia, Report No. AEEP-3435-115-70U, April 1970.

APPENDIXES
I. ILLUSTRATIONS
II. TABLES

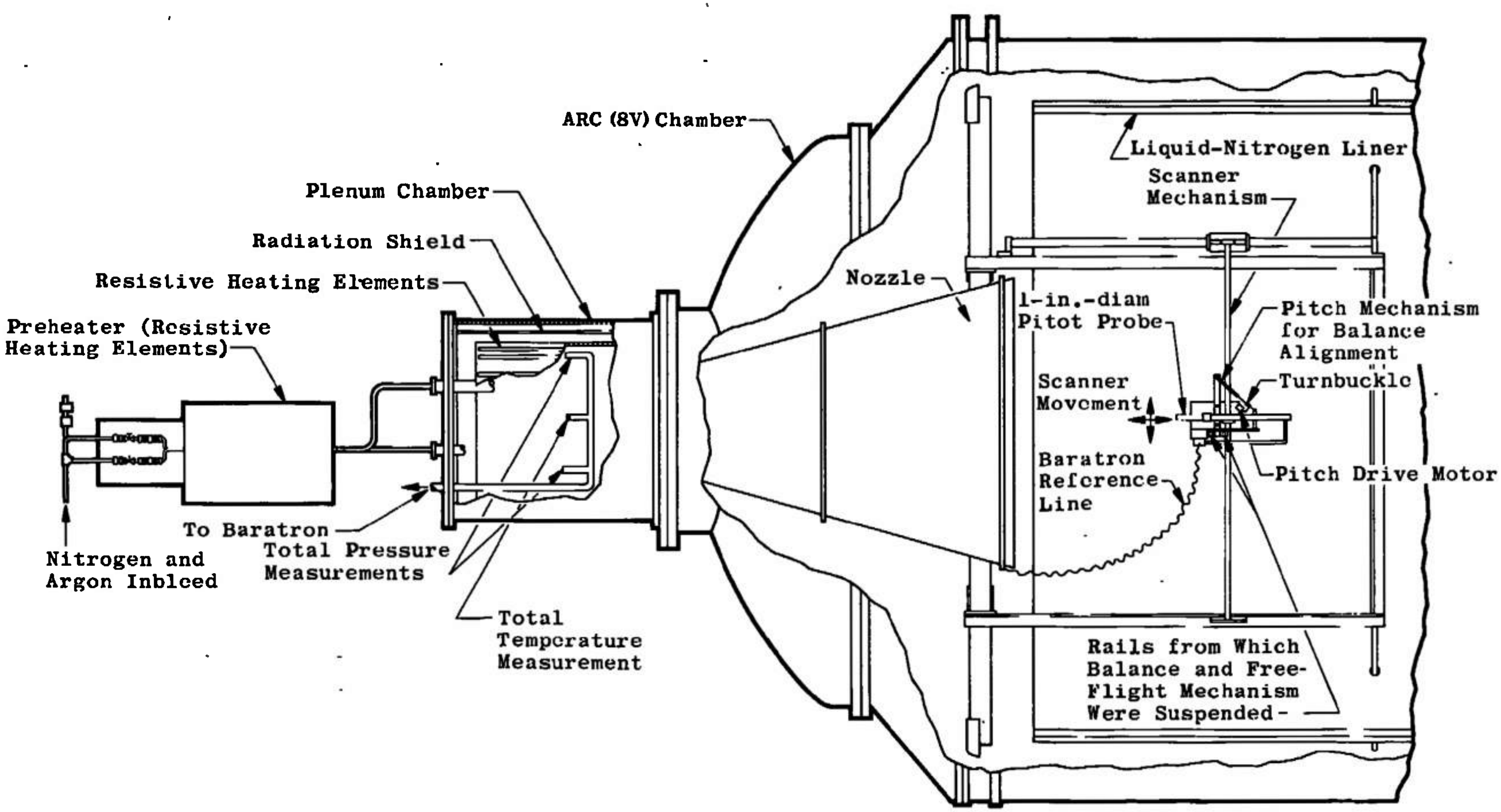

Fig. 1 Schematic of Low-Density Tunnel, ARC (10V)

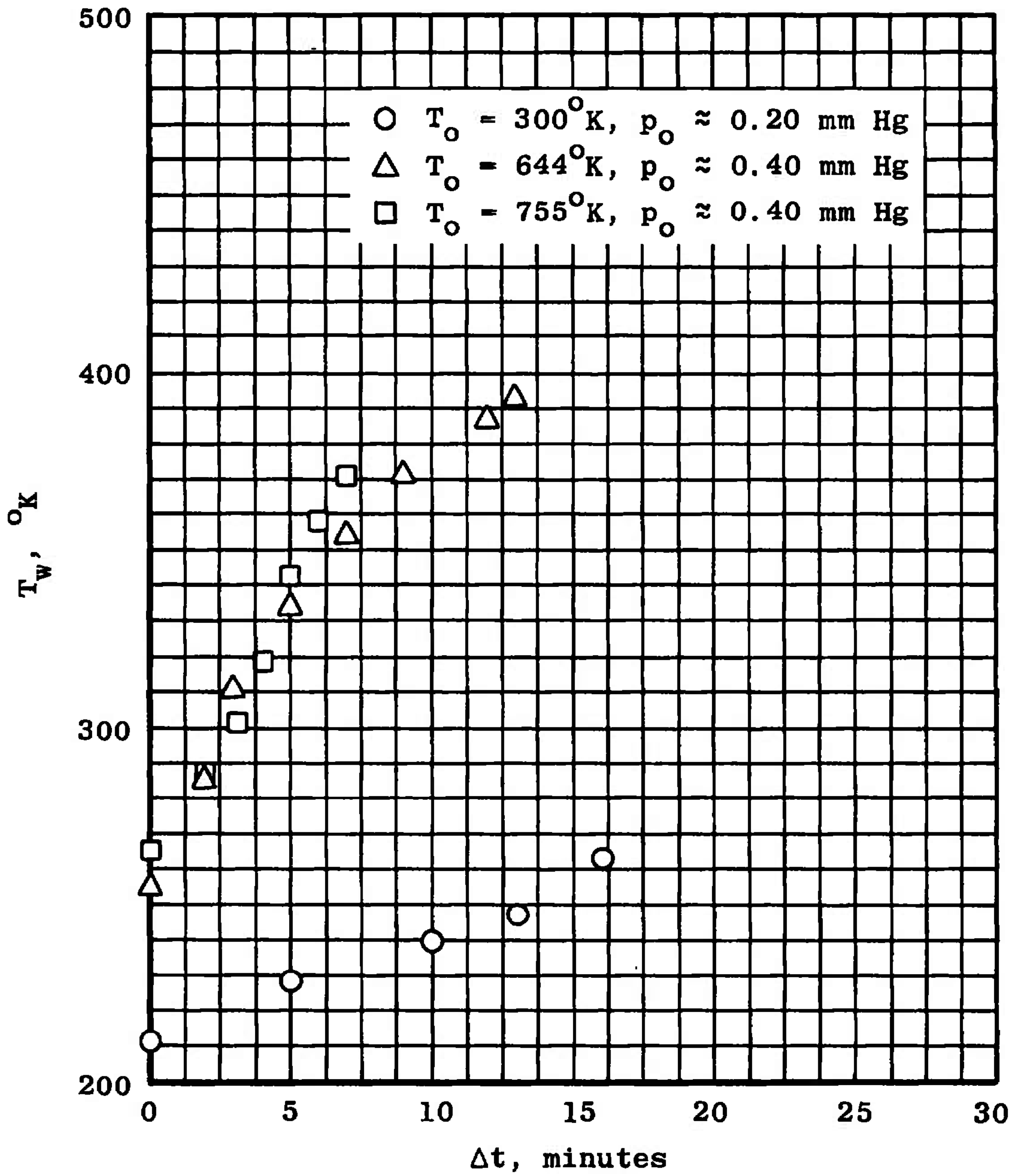

Fig. 2 Change in Sphere Wall Temperature with Time

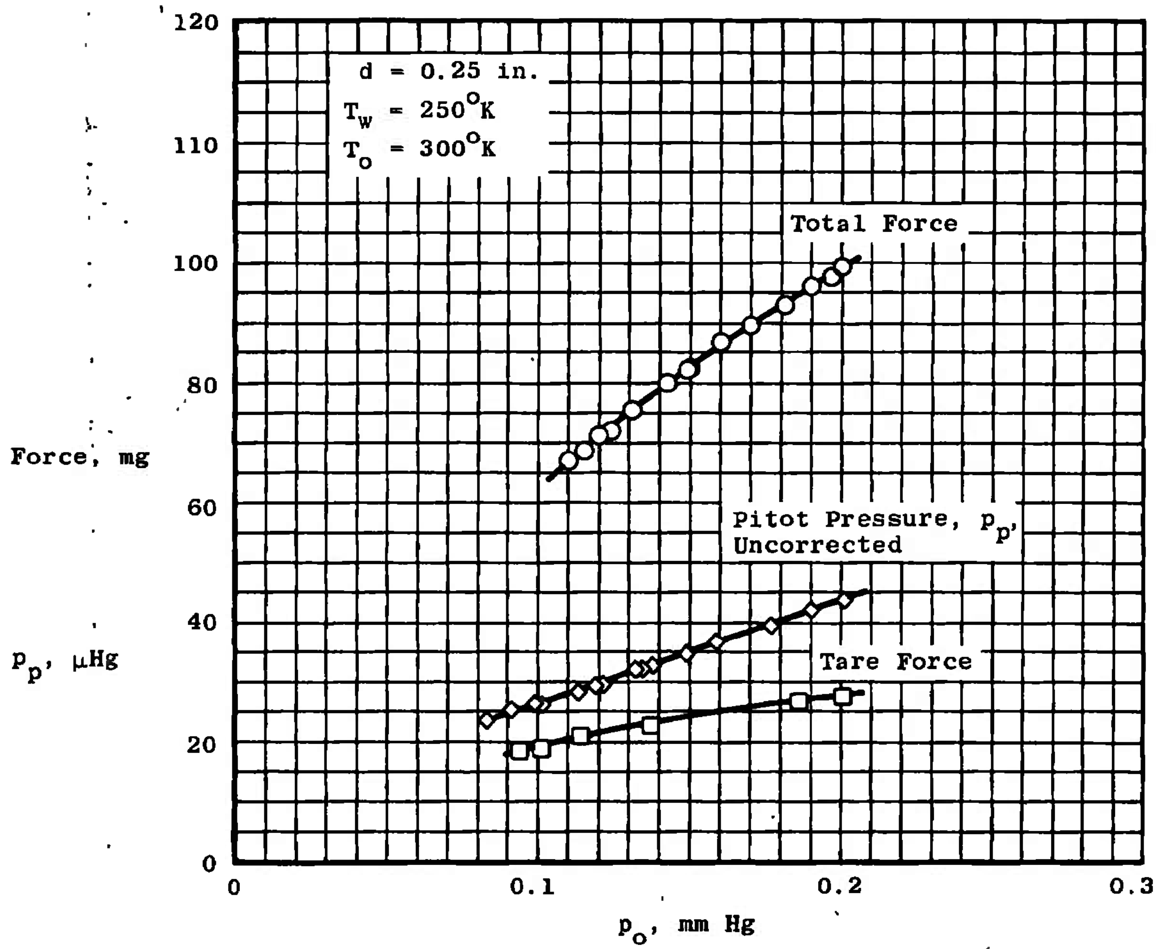

Fig. 3 Force and Pitot Pressure Measurements 10 in. Downstream of Mach 3 Nozzle Exit

Sym	M_∞	T_w/T_∞	Kn_∞	T_o, ^oK
○	3.308 to 3.450	2.368 to 2.847	0.555 to 0.894	300
△	3.550 to 3.594	1.417 to 2.143	0.805 to 1.168	641 to 644
□	3.603 to 3.633	1.204 to 1.778	0.998 to 1.290	750 to 755

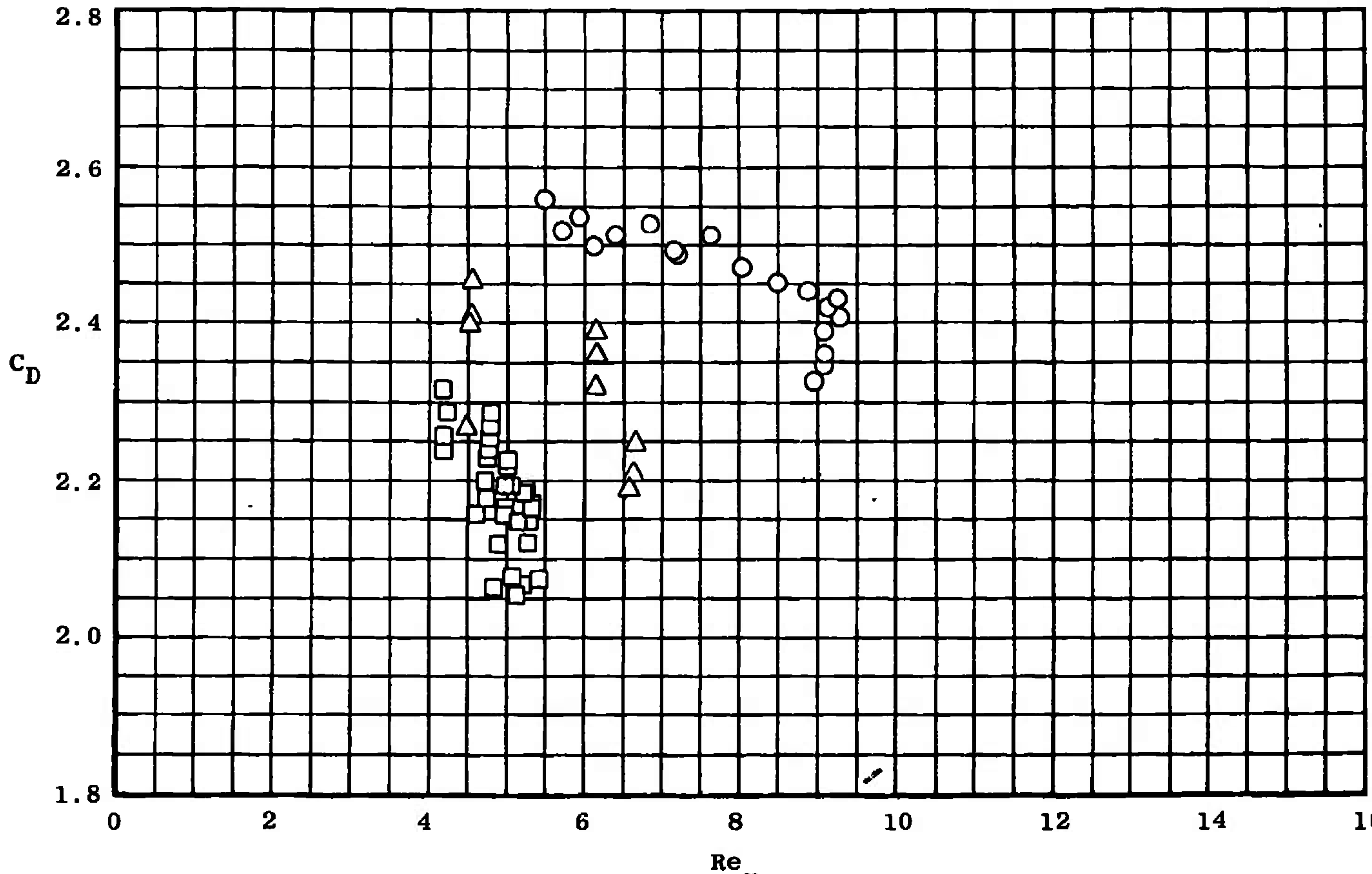

Fig. 4 Summary of Experimental Sphere Drag Data

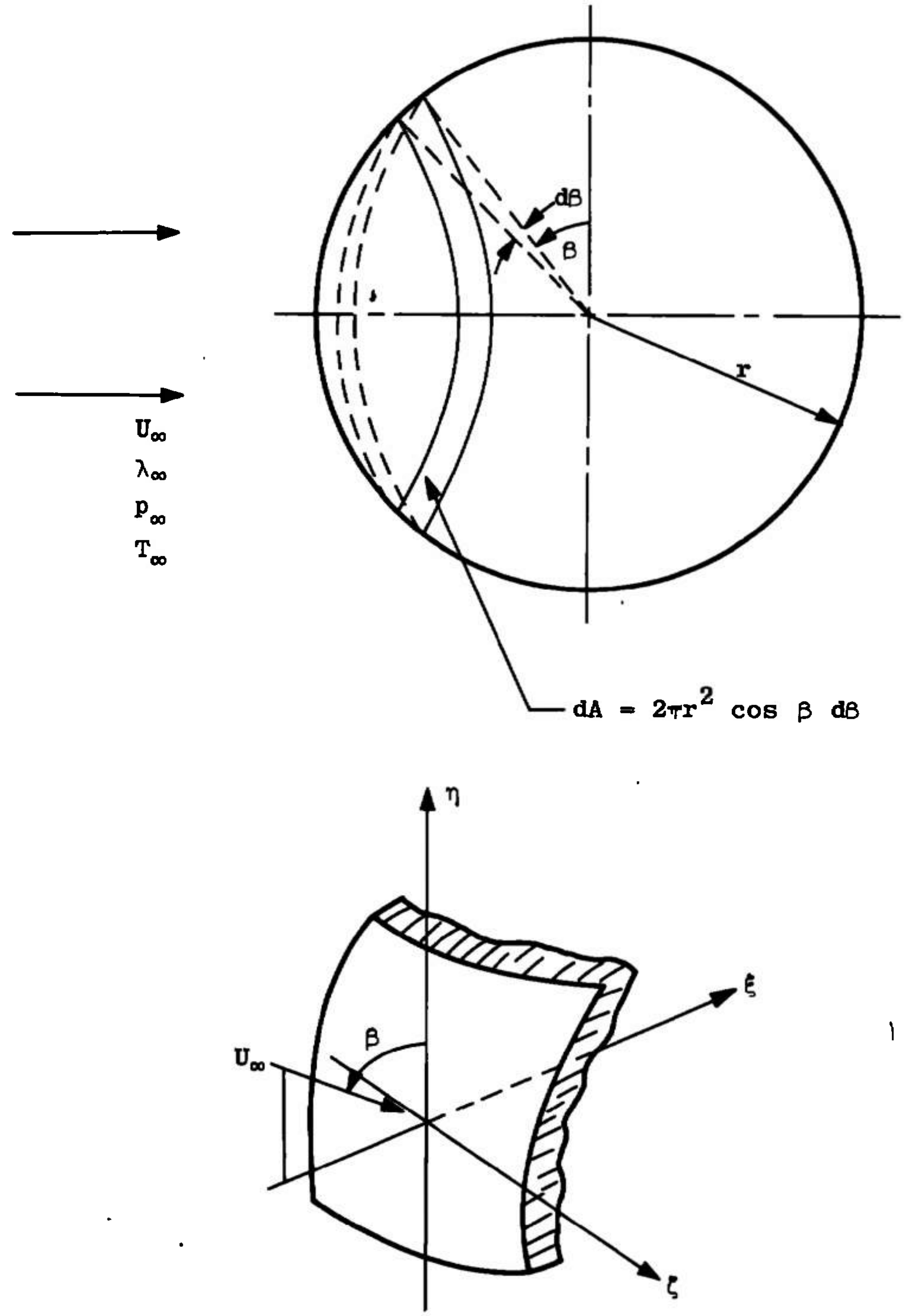

Fig. 5 Coordinate System

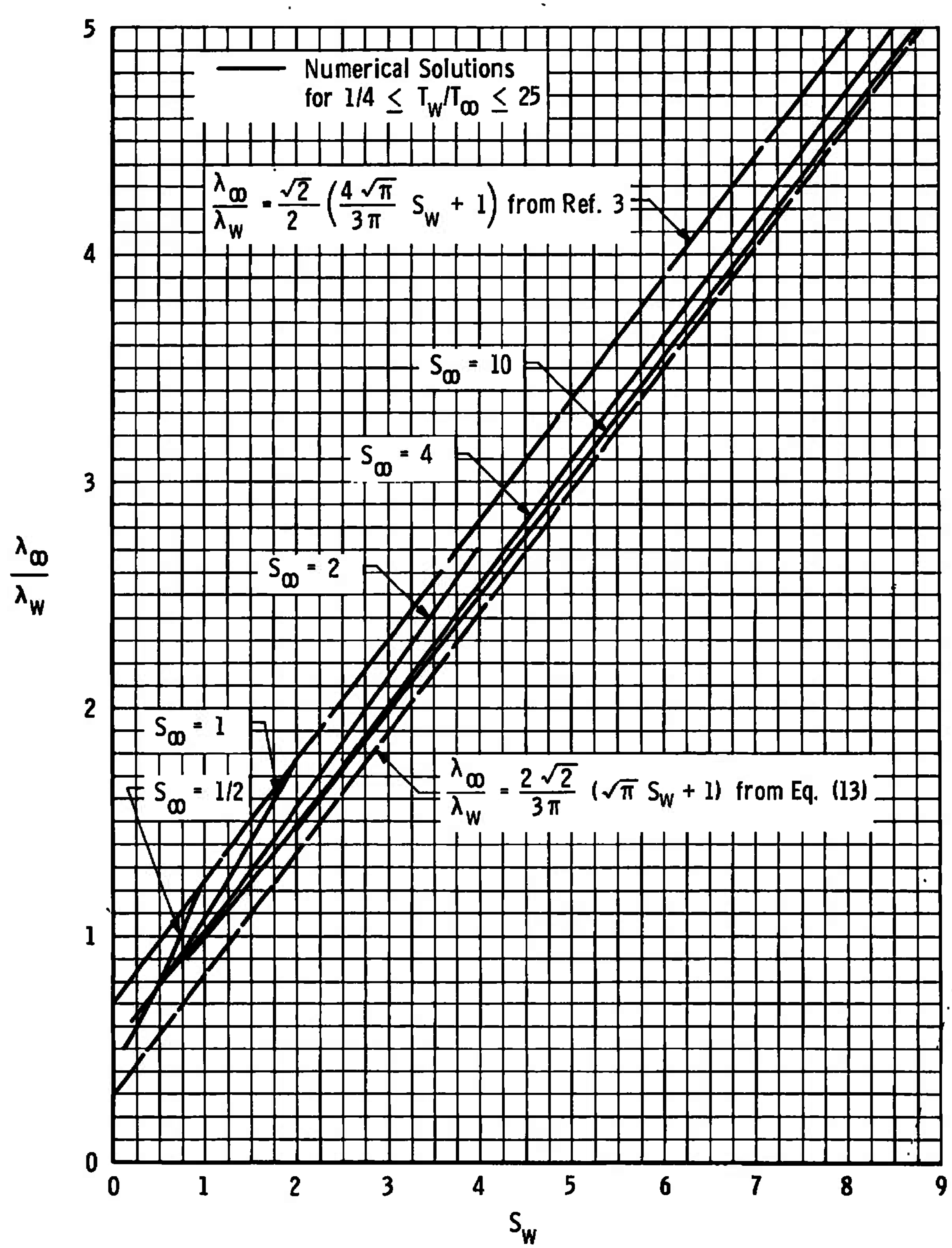

Fig. 6 Numerical and Approximate Analytical Solutions for λ_∞/λ_w

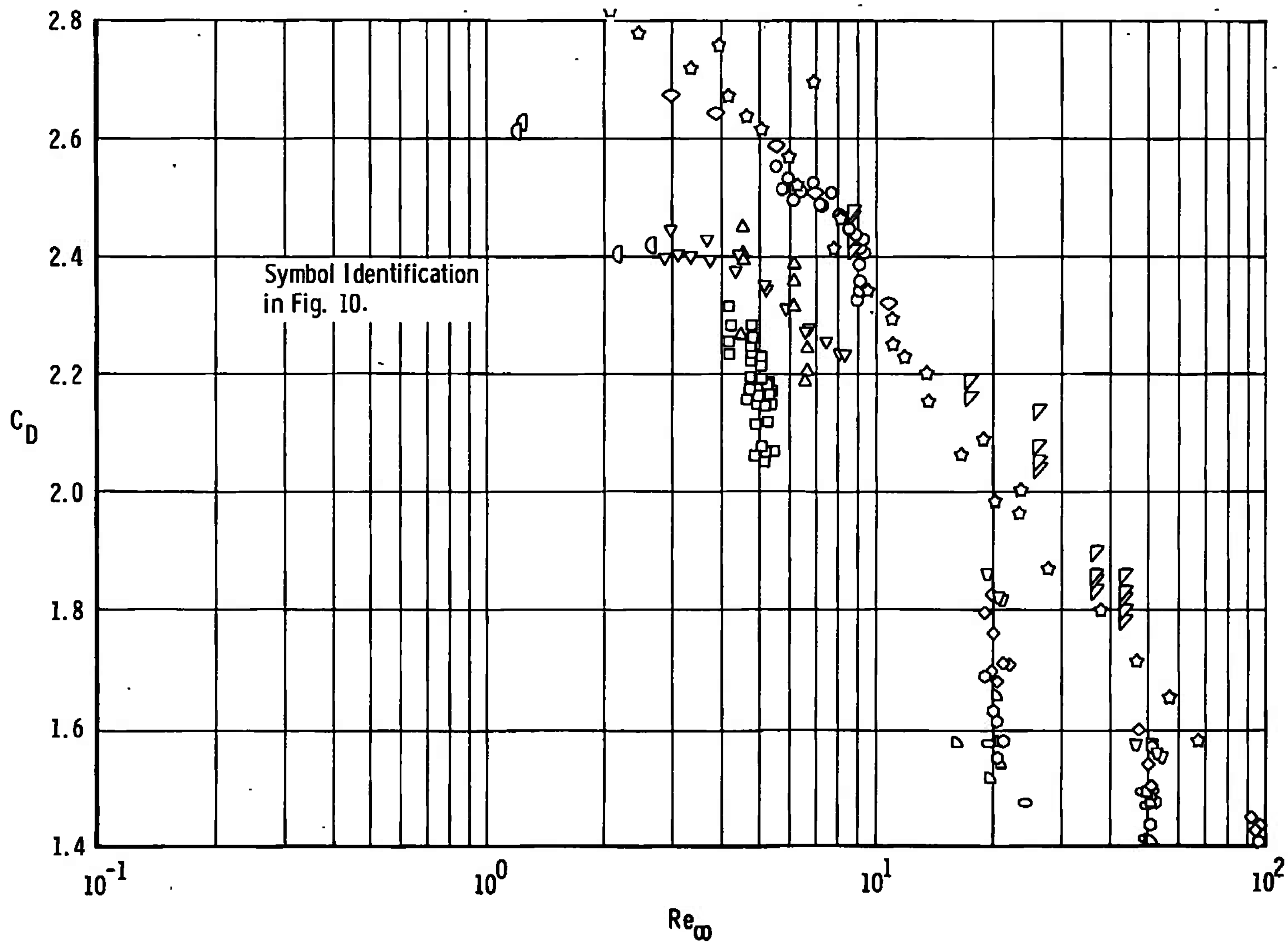

Fig. 7 Sphere Drag Data in Terms of C_D and Re_∞

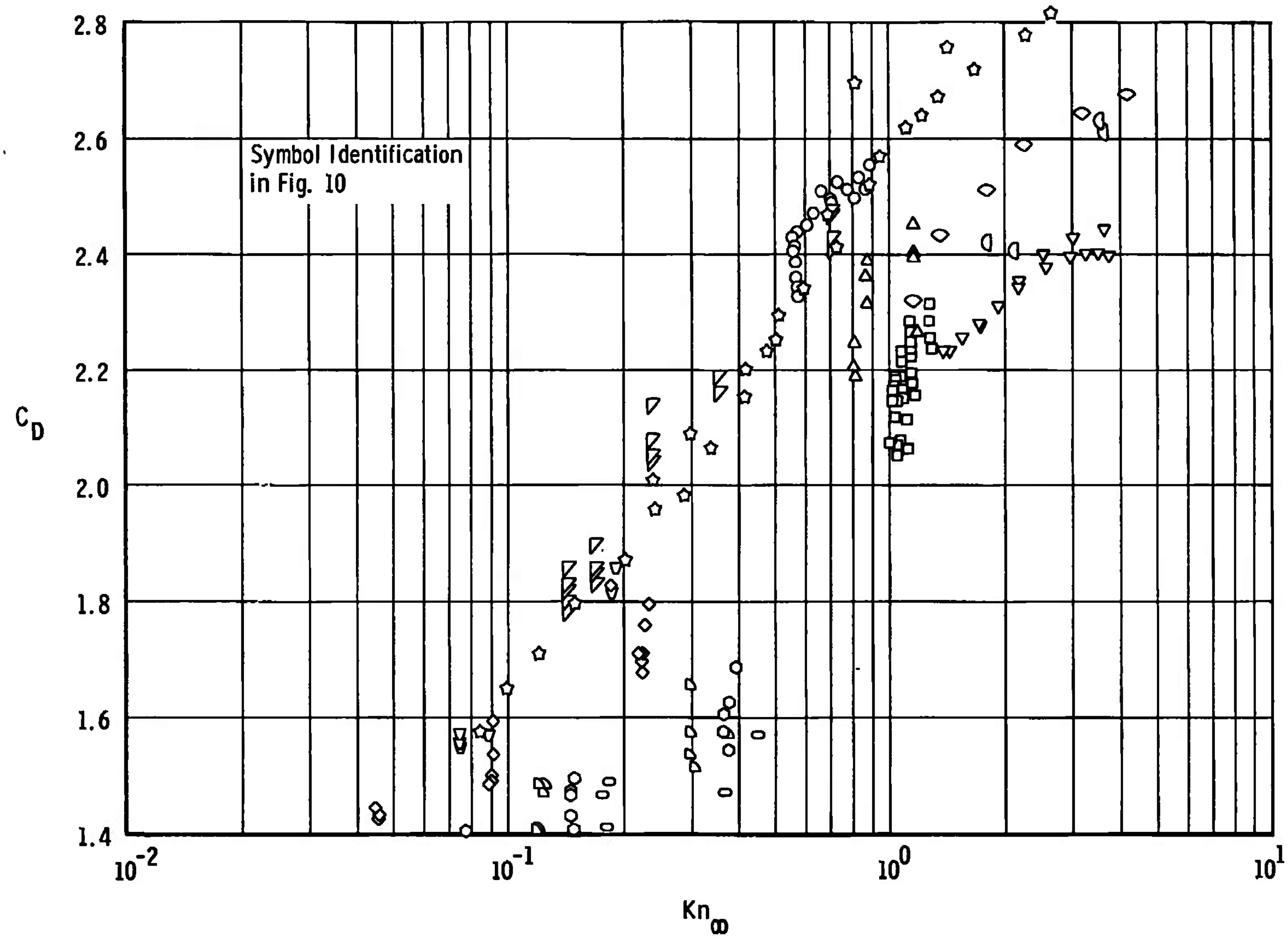

Fig. 8 Sphere Drag Data in Terms of C_D and Kn_{∞}

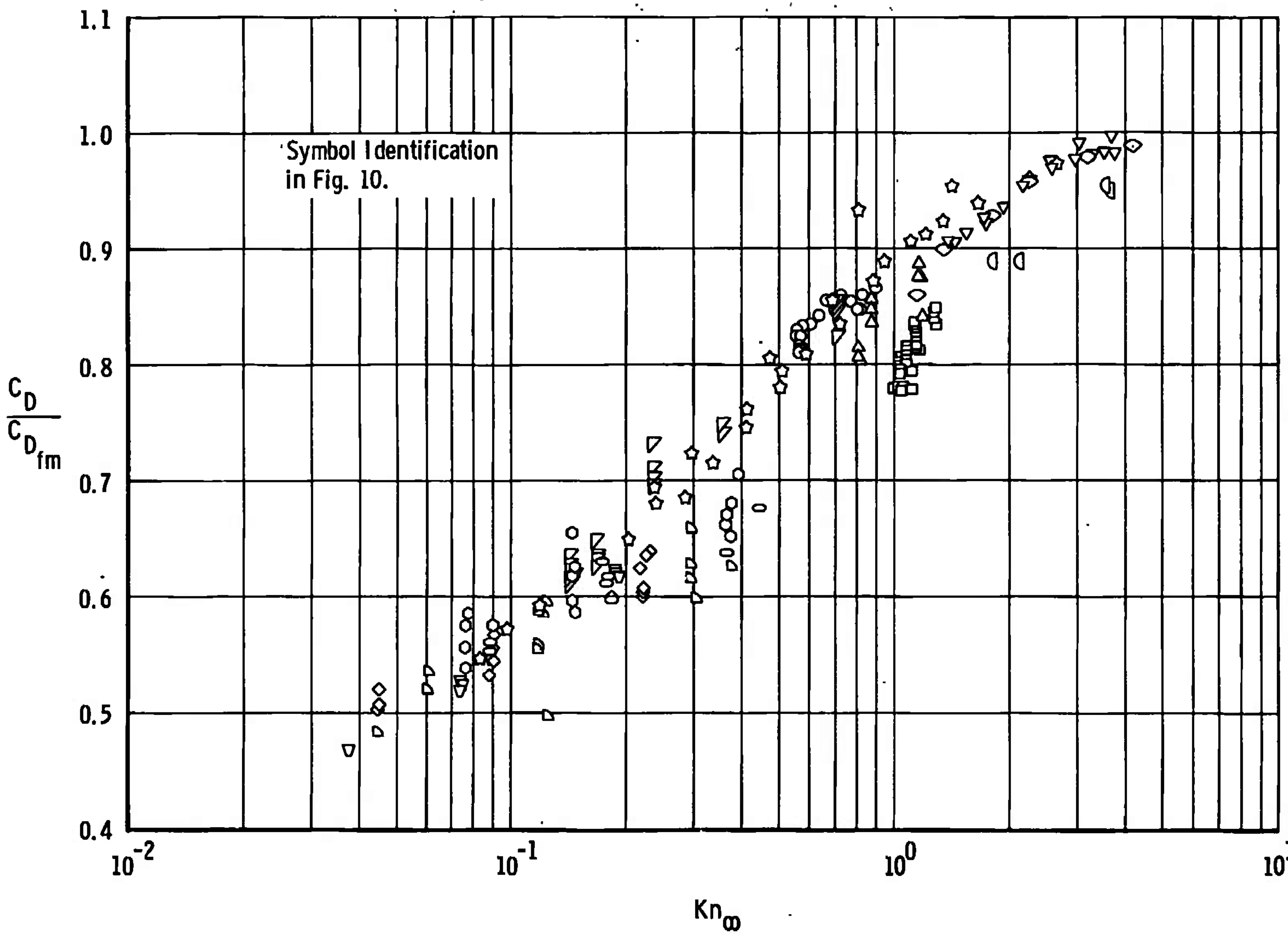

Fig. 9 Sphere Drag Data in Terms of $C_D/C_{D\,fm}$ and Kn_∞

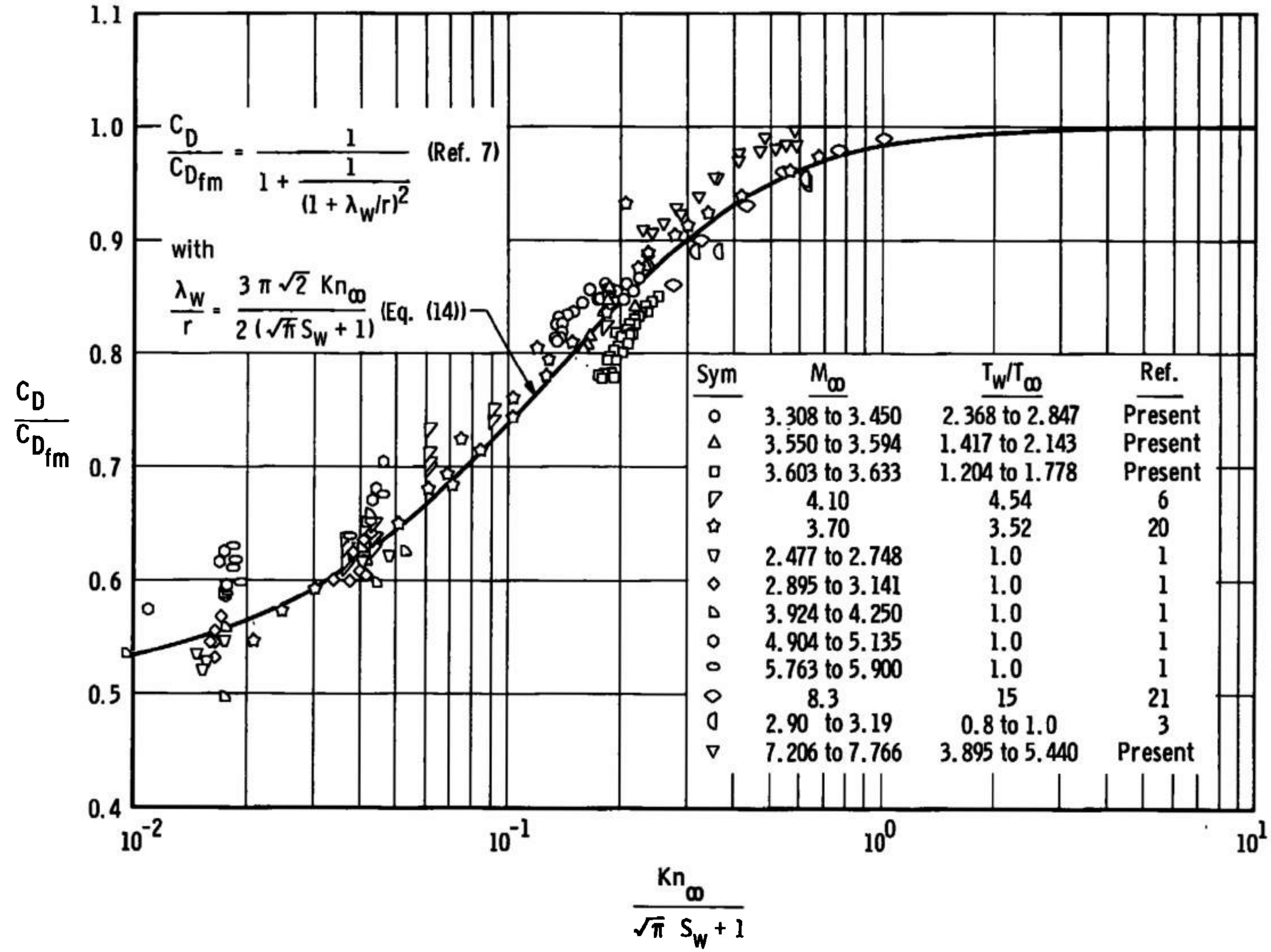

Fig. 10 Sphere Drag Data in Terms of $C_D/C_{D_{fm}}$ and $Kn_\infty/(\sqrt{\pi}\,S_w + 1)$

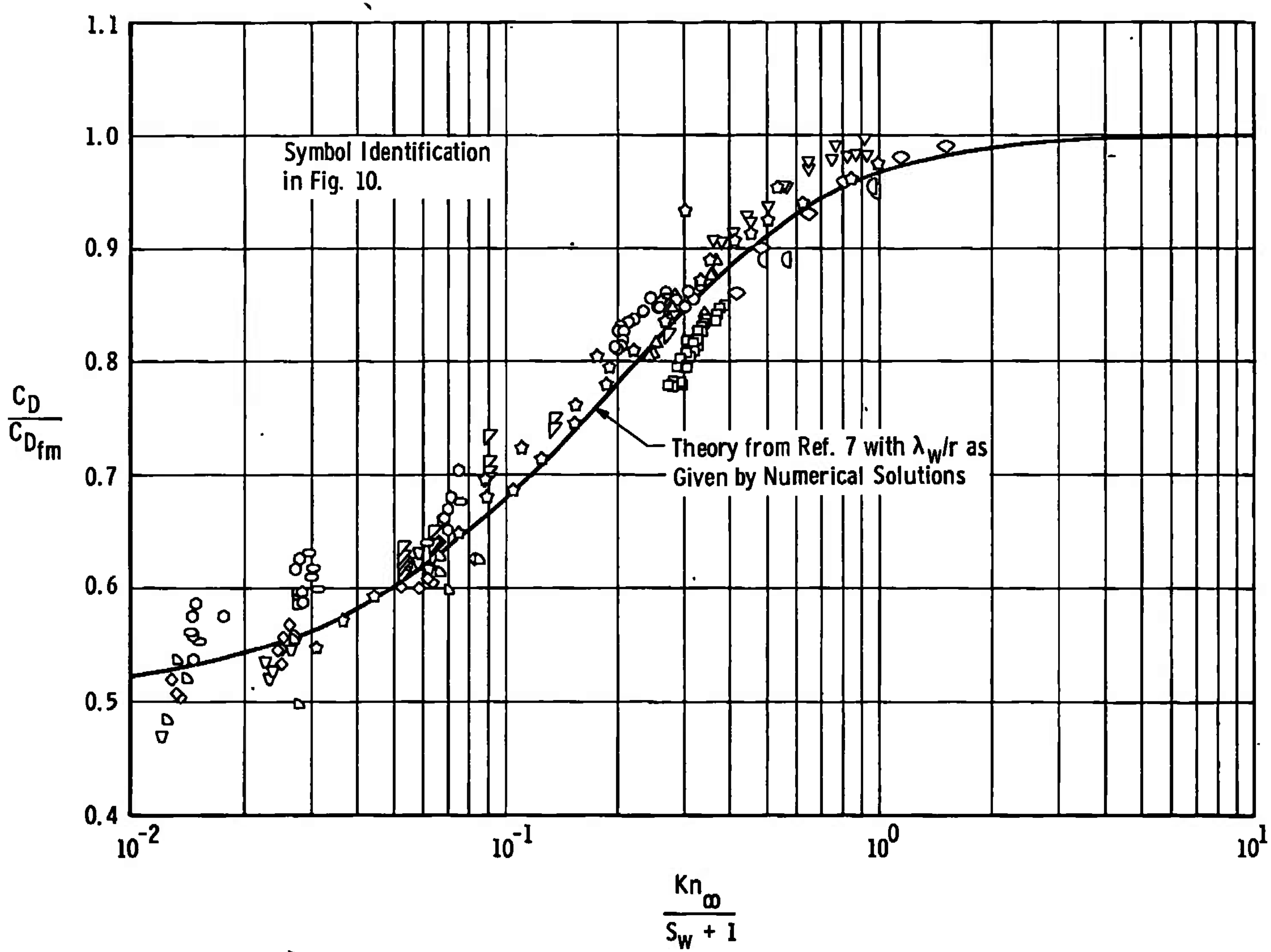

Fig. 11 Sphere Drag Data According to Correlation Provided by Numerical Solutions for λ_w/λ_∞

Sym	M_∞	Kn_∞	Ref.
○	3.441 to 3.450	0.555 to 0.573	Present
□	3.613 to 3.617	1.126 to 1.166	Present
◇	3.603 to 3.604	1.276 to 1.290	Present
■	3.624 to 3.633	0.998 to 1.054	Present
0	3.617 to 3.620	1.076 to 1.115	Present
◤	4.10	0.706	6
◸	4.10	0.353	6
★	3.70	0.510 to 0.893	20
☆	3.70	0.238 to 0.503	20
⌂	3.978 to 5.135	0.293 to 0.376	1
——	$S_\infty = \sqrt{\frac{\gamma}{2}} M_\infty = 3$	Indicated	7 (Theory)

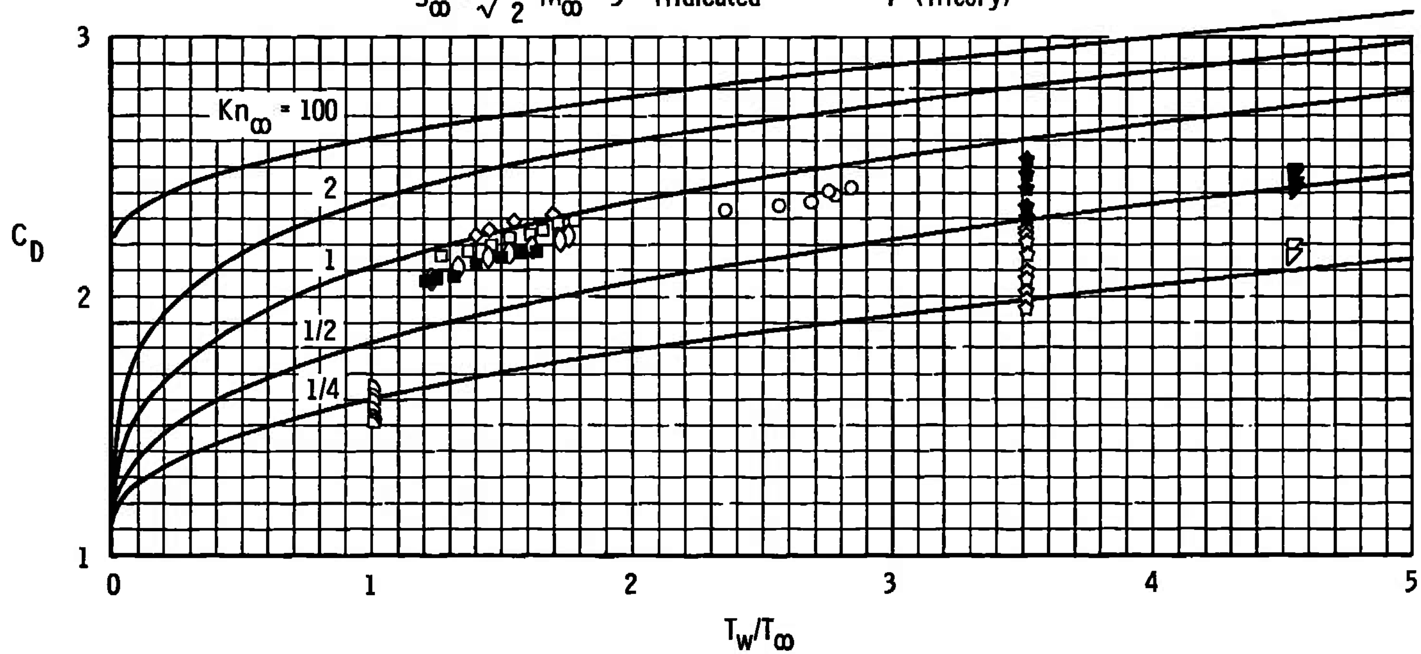

Fig. 12 Effect of Wall Temperature on Sphere Drag

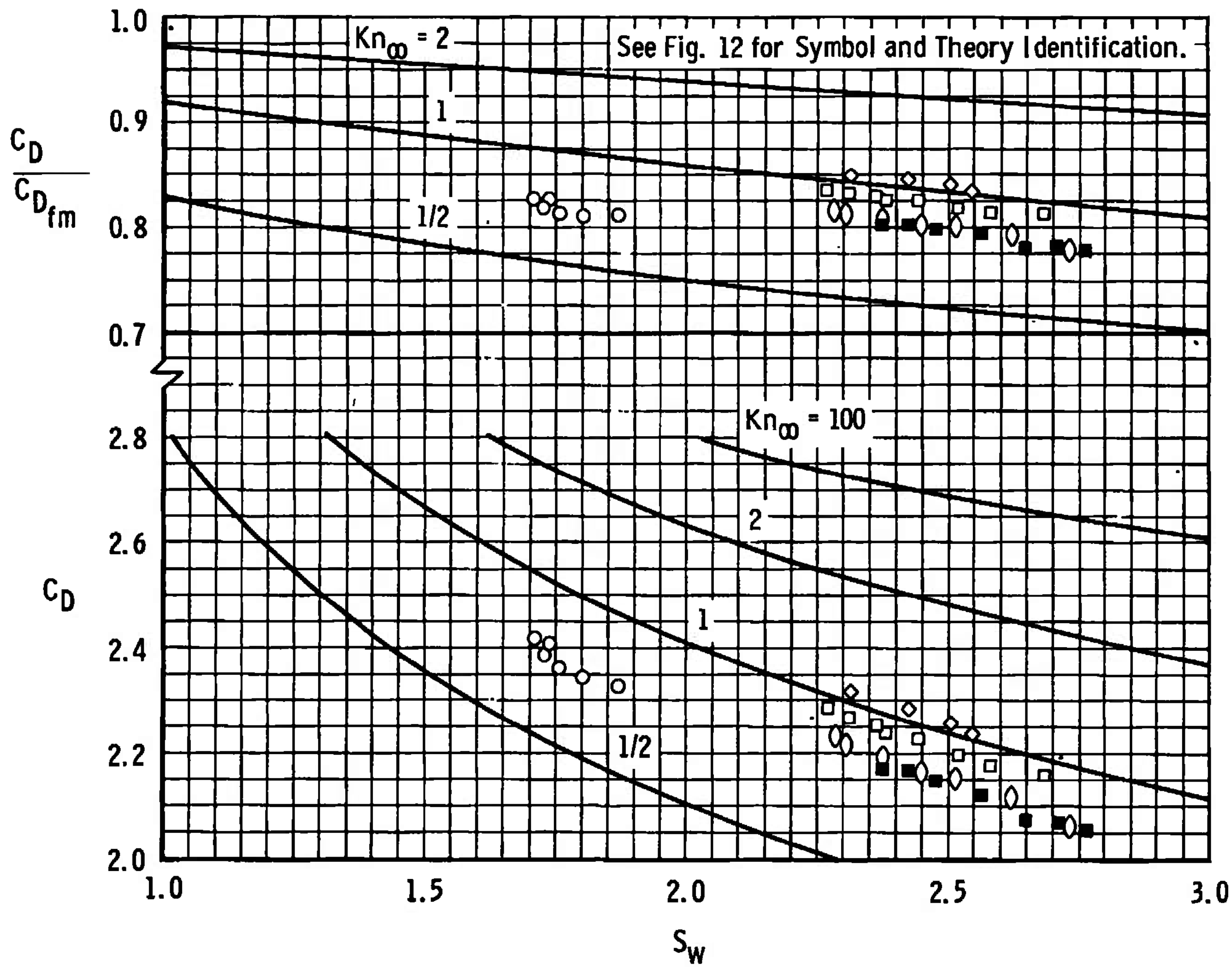

Fig. 13 Variation of Present Drag Results with Wall Speed Ratio

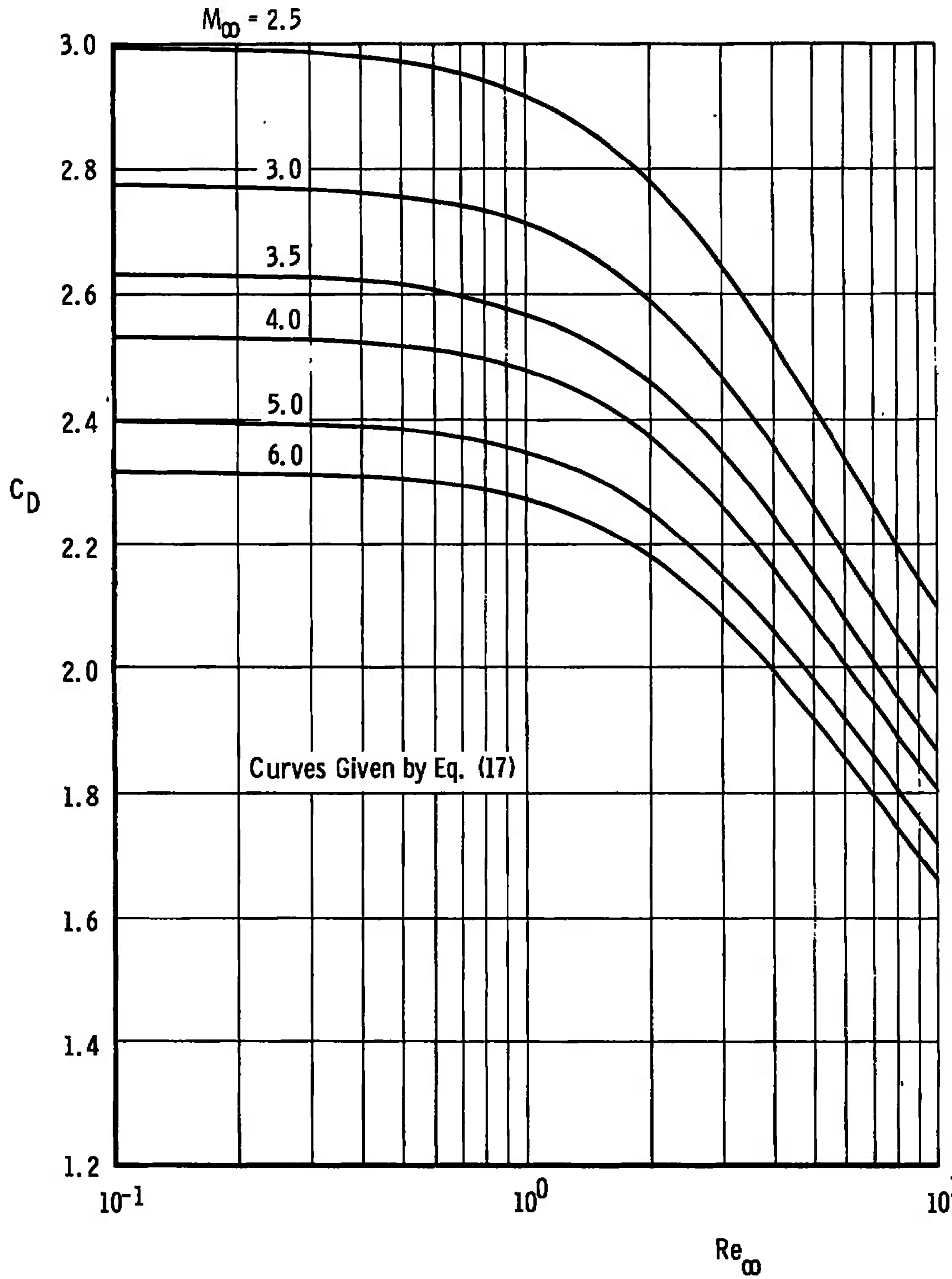

Fig. 14 Sphere Drag Coefficients for γ = 1.4 and T_w/T_∞ = 1

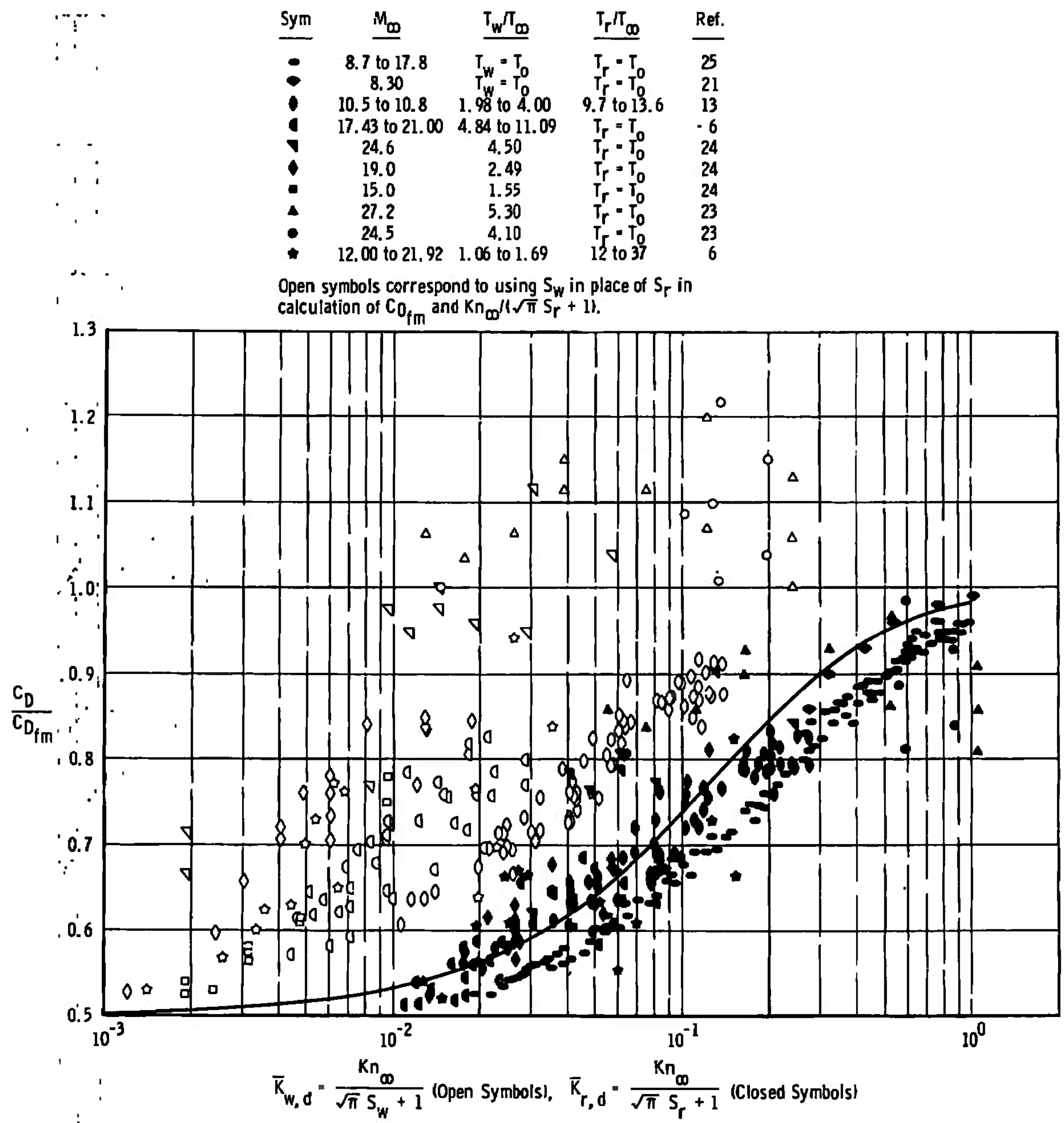

Fig. 15 Correlation of High Enthalpy Hypersonic Sphere Drag Data

TABLE I
SPHERE DRAG AND FLOW CONDITIONS IN THE MACH 3 NOZZLE

M_∞	Re_∞	Kn_∞	T_w/T_∞	S_w	C_D	$C_D/C_{D_{fm}}$	p_o, mm Hg	T_o, °K	T_w, °K	$\overline{K}_{w,d}$
3.450	9.274	0.5546	2.753	1.740	2.406	0.8263	0.2000	300.0	244.27	0.1358
3.441	8.947	0.5734	2.368	1.871	2.327	0.8119	0.1920		210.94	0.1329
3.445	9.070	0.5662	2.559	1.802	2.343	0.8108	0.1950		227.60	0.1350
3.445	9.070	0.5662	2.684	1.759	2.360	0.8123	0.1950		238.72	0.1375
3.445	9.070	0.5662	2.778	1.729	2.388	0.8186	0.1950		247.05	0.1393
3.446	9.111	0.5638	2.841	1.710	2.417	0.8265	0.1960		252.60	0.1399
3.383	7.167	0.7038	2.769	1.701	2.491	0.8484	0.1490		252.60	0.1753
3.338	6.112	0.8143	2.725	1.692	2.498	0.8478	0.1240		253.16	0.2036
3.308	5.514	0.8944	2.655	1.698	2.557	0.8671	0.1100		249.83	0.2230
3.319	5.728	0.8639	2.668	1.700	2.517	0.8545	0.1150		249.83	0.2152
3.330	5.942	0.8356	2.674	1.704	2.534	0.8610	0.1200		249.27	0.2078
3.352	6.409	0.7797	2.698	1.707	2.511	0.8547	0.1310		249.27	0.1937
3.372	6.873	0.7314	2.726	1.709	2.526	0.8605	0.1420		249.83	0.1816
3.385	7.208	0.7000	2.747	1.709	2.487	0.8480	0.1500		250.38	0.1738
3.400	7.626	0.6647	2.764	1.711	2.509	0.8563	0.1600		250.38	0.1648
3.414	8.040	0.6330	2.792	1.709	2.470	0.8433	0.1700		251.49	0.1571
3.428	8.495	0.6016	2.821	1.708	2.449	0.8364	0.1810		252.60	0.1494
3.439	8.865	0.5783	2.834	1.709	2.439	0.8338	0.1900		252.60	0.1435
3.450	9.274	0.5546	2.847	1.711	2.430	0.8311	0.2000		252.60	0.1375
3.593	6.571	0.8152	1.683	2.317	2.188	0.8029	0.4400	641.5	301.49	0.1596
3.594	6.627	0.8085	1.768	2.261	2.207	0.8062	0.4440	641.5	316.49	0.1614
3.594	6.655	0.8053	1.877	2.195	2.245	0.8153	0.4460	641.5	335.94	0.1646
3.586	6.157	0.8685	1.964	2.141	2.316	0.8367	0.4130	644.3	354.27	0.1811
3.587	6.171	0.8666	2.057	2.092	2.360	0.8486	0.4140	644.3	370.94	0.1840
3.586	6.157	0.8685	2.143	2.050	2.389	0.8557	0.4130	644.3	386.49	0.1875
3.550	4.474	1.183	1.417	2.495	2.264	0.8403	0.2870	633.2	254.83	0.2182
3.551	4.532	1.168	1.668	2.301	2.397	0.8769	0.2910	633.2	299.83	0.2301
3.552	4.562	1.161	1.730	2.259	2.406	0.8770	0.2930	633.2	310.94	0.2320
3.552	4.562	1.161	1.823	2.201	2.452	0.8895	0.2930	633.2	327.60	0.2368
3.623	5.034	1.073	1.327	2.632	2.077	0.7807	0.4240	755.6	276.49	0.1894

TABLE I (Concluded)

M_∞	Re_∞	Kn_∞	T_w/T_∞	S_w	C_D	$C_D/C_{D_{fm}}$	p_o, mm Hg	T_o, °K	T_w, °K	$\overline{K}_{w,d}$
3.623	5.023	1.075	1.438	2.527	2.191	0.8179	0.4230	755.6	299.83	0.1962
3.626	5.177	1.044	1.526	2.456	2.146	0.7970	0.4370		317.60	0.1951
3.627	5.209	1.038	1.612	2.390	2.181	0.8060	0.4400		335.38	0.1982
3.628	5.242	1.032	1.663	2.354	2.186	0.8057	0.4430		345.94	0.1995
3.613	4.622	1.166	1.268	2.684	2.157	0.8132	0.3870		265.38	0.2024
3.615	4.711	1.144	1.373	2.581	2.174	0.8140	0.3950		287.05	0.2052
3.616	4.734	1.139	1.442	2.519	2.196	0.8190	0.3970		301.49	0.2084
3.616	4.756	1.134	1.528	2.448	2.225	0.8254	0.3990		319.27	0.2123
3.617	4.779	1.128	1.613	2.382	2.238	0.8264	0.4010		337.05	0.2160
3.617	4.779	1.128	1.640	2.363	2.251	0.8298	0.4010		342.60	0.2175
3.617	4.790	1.126	1.714	2.311	2.266	0.8321	0.4020		358.16	0.2209
3.617	4.790	1.126	1.778	2.269	2.284	0.8357	0.4020		371.49	0.2242
3.603	4.165	1.290	1.401	2.547	2.235	0.8346	0.3450	752.8	293.16	0.2339
3.604	4.188	1.283	1.451	2.503	2.257	0.8403	0.3470		303.72	0.2360
3.604	4.211	1.276	1.547	2.424	2.283	0.8453	0.3490		323.72	0.2409
3.603	4.176	1.286	1.698	2.314	2.315	0.8497	0.3460		355.38	0.2522
3.617	4.836	1.115	1.227	2.732	2.061	0.7794	0.4040		255.38	0.1908
3.618	4.892	1.103	1.334	2.621	2.115	0.7943	0.4090		277.60	0.1953
3.619	4.961	1.087	1.452	2.513	2.151	0.8018	0.4130	750.0	300.94	0.1994
3.620	4.995	1.080	1.528	2.450	2.163	0.8028	0.4160		316.49	0.2022
3.620	5.006	1.078	1.622	2.378	2.191	0.8089	0.4170		335.94	0.2067
3.620	5.017	1.076	1.724	2.307	2.216	0.8134	0.4180		357.05	0.2114
3.620	5.017	1.076	1.759	2.284	2.232	0.8177	0.4180		364.27	0.2131
3.624	5.125	1.054	1.204	2.764	2.051	0.7771	0.4300		249.83	0.1787
3.626	5.191	1.041	1.253	2.710	2.067	0.7807	0.4360	752.8	259.83	0.1794
3.627	5.257	1.029	1.401	2.564	2.120	0.7935	0.4420		290.38	0.1855
3.629	5.301	1.021	1.501	2.478	2.147	0.7987	0.4460		310.94	0.1893
3.629	5.312	1.019	1.568	2.425	2.164	0.8020	0.4470		324.83	0.1923
3.629	5.232	1.017	1.635	2.374	2.170	0.8011	0.4480		338.72	0.1952
3.633	5.426	0.9982	1.316	2.650	2.072	0.7800	0.4600	755.6	273.16	0.1752

TABLE II
SPHERE DRAG AND FLOW CONDITIONS IN THE MACH 6 NOZZLE

M_∞	Re_∞	Kn_∞	T_w/T_∞	S_w	C_D	$C_D/C_{D_{fm}}$	p_o, mm Hg	T_o, °K	T_w, °K	$\bar{K}_{w,d}$
7.223	2.944	3.658	4.087	2.989	2.446	0.9984	1.514	800.0	286.00	0.5808
7.383	3.656	3.011	4.395	2.947	2.432	0.9913	1.991		295.50	0.4839
7.504	4.432	2.524	4.689	2.899	2.402	0.9772	2.518		306.00	0.4112
7.590	5.175	2.186	4.885	2.873	2.351	0.9553	3.030		312.10	0.3589
7.647	5.885	1.937	5.040	2.850	2.311	0.9381	3.513		317.70	0.3202
7.692	6.606	1.736	5.184	2.827	2.277	0.9233	4.005		323.20	0.2888
7.739	7.443	1.550	5.333	2.804	2.258	0.9145	4.585		328.80	0.2597
7.759	8.078	1.432	5.440	2.783	2.238	0.9055	5.010		333.80	0.2414
7.206	2.852	3.767	3.895	3.055	2.400	0.9829	1.457		273.80	0.5873
7.264	3.080	3.517	4.025	3.029	2.405	0.9842	1.607		278.80	0.5521
7.312	3.315	3.289	4.139	3.007	2.401	0.9817	1.760		283.20	0.5195
7.395	3.714	2.968	4.308	2.981	2.397	0.9790	2.031		288.80	0.4724
7.495	4.364	2.560	4.509	2.953	2.378	0.9703	2.471		294.90	0.4107
7.590	5.196	2.178	4.693	2.931	2.343	0.9556	3.042		299.90	0.3515
7.702	6.675	1.720	4.956	2.895	2.280	0.9283	4.060		308.25	0.2806
7.766	8.316	1.392	5.122	2.871	2.234	0.9084	5.169		313.80	0.2287

UNCLASSIFIED

Security Classification

DOCUMENT CONTROL DATA - R & D

(Security classification of title, body of abstract and indexing annotation must be entered when the overall report is classified)

1. ORIGINATING ACTIVITY *(Corporate author)* Arnold Engineering Development Center ARO, Inc., Operating Contractor Arnold Air Force Station, Tennessee	2a. REPORT SECURITY CLASSIFICATION UNCLASSIFIED 2b. GROUP N/A

3. REPORT TITLE

LOW-DENSITY SUPERSONIC SPHERE DRAG WITH VARIABLE WALL TEMPERATURE

4. DESCRIPTIVE NOTES *(Type of report and inclusive dates)*

Final Report - December 1969 to September 9, 1970

5. AUTHOR(S) *(First name, middle initial, last name)*

D. L. Whitfield and H. K. Smithson, ARO, Inc.

6. REPORT DATE	7a. TOTAL NO. OF PAGES	7b. NO OF REFS
July 1971	44	25

8a. CONTRACT OR GRANT NO. F40600-71-C-0002 b. PROJECT NO. 6682 c. Program Element 65701F d.	9a. ORIGINATOR'S REPORT NUMBER(S) AEDC-TR-71-83 9b. OTHER REPORT NO(S) *(Any other numbers that may be assigned this report)* ARO-VKF-TR-71-39

10 DISTRIBUTION STATEMENT

Approved for public release; distribution unlimited.

11. SUPPLEMENTARY NOTES	12. SPONSORING MILITARY ACTIVITY
Available in DDC	Air Force Cambridge Research Lab. (CRER), L. G. Hanscom Field, Bedford Mass. 01730

13. ABSTRACT

Force measurements were made to investigate the effect of wall temperature on sphere drag in low-density supersonic flow. Drag data were obtained by fixing flow conditions and changing only the sphere wall temperature. Conditions covered in the experiment include $3.3 < M_\infty < 3.7$, $4.0 < Re_\infty < 10.0$, $0.5 < Kn_\infty < 1.3$, and $1.2 < T_w/T_\infty < 3.0$. A means of correlating drag data in transition flow is suggested, and its validity assessed by applying the correlation parameter to this and several other sets of experimental data.

DD FORM 1 NOV 65 1473

UNCLASSIFIED

Security Classification

UNCLASSIFIED
Security Classification

14. KEY WORDS	LINK A		LINK B		LINK C	
	ROLE	WT	ROLE	WT	ROLE	WT
1 spheres -- Drag						
supersonic flow						
drag						

2 Spheres - Supersonic flow

AFSC
Arnold AFS Tenn

UNCLASSIFIED
Security Classification